Article

Current Biology

The burning glass effect of water droplets triggers a high light-induced calcium response in the chloroplast stroma

Graphical abstract

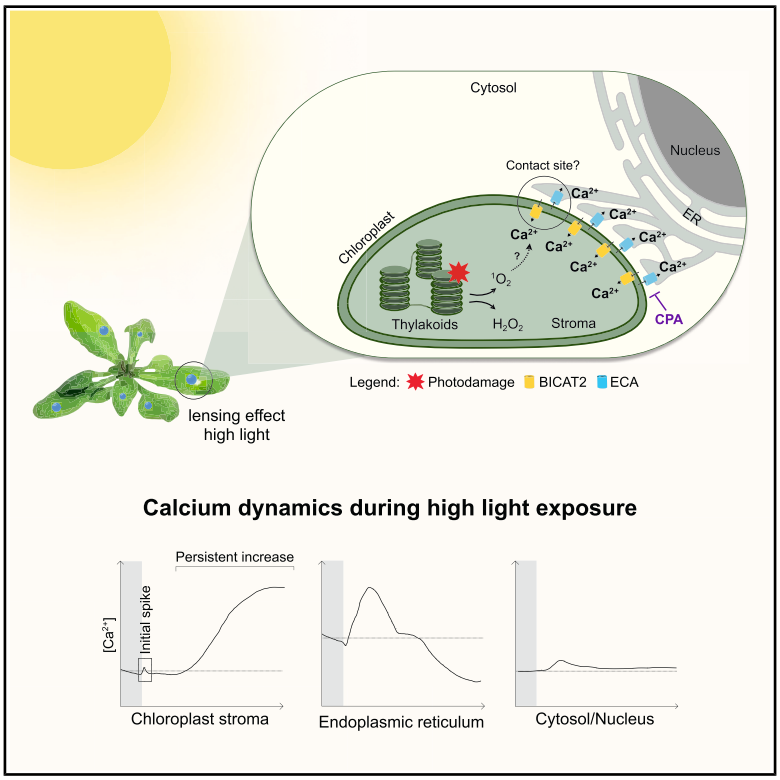

Authors

Dominic Kuang, Shanna Romand, Anna S. Zvereva, ..., Markus Teige, Alex Costa, Simon Stael

Correspondence

simon.stael@slu.se

In brief

Excessive light exposure can harm plants. Searching for potential acclimation mechanisms, Kuang et al. show that high light triggers Ca^{2+} responses in the chloroplast stroma, cytosol, and ER of *Arabidopsis thaliana*, dependent on photodamage, ROS formation, and temperature, revealing a surprising connection between ER and chloroplast Ca^{2+} pools.

Highlights

- High light triggers Ca^{2+} responses in the chloroplast stroma, cytosol, and ER
- Photodamage and singlet oxygen contribute to the stromal Ca^{2+} response
- The stromal response is light driven but enhanced by temperature increase
- Ca^{2+} transfer between chloroplast and ER is perturbed by high light

Kuang et al., 2025, Current Biology *35*, 2642–2658
June 9, 2025
https://doi.org/10.1016/j.cub.2025.04.065

CellPress

CellPress
OPEN ACCESS

Current Biology

Article

The burning glass effect of water droplets triggers a high light-induced calcium response in the chloroplast stroma

Dominic Kuang,[1,12] Shanna Romand,[1,12] Anna S. Zvereva,[2] Bianca Maria Orlando Marchesano,[3] Matteo Grenzi,[3] Stefano Buratti,[3] Qun Yang,[1] Ke Zheng,[4] Dimitra Valadorou,[5,6] Evelien Mylle,[7,8] Zuzana Benedikty,[9] Martin Trtílek,[9] Maria Tenje,[5,6] Cornelia Spetea,[10] Daniël Van Damme,[7,8] Bernhard Wurzinger,[2] Markus Schwarzländer,[4] Markus Teige,[2] Alex Costa,[3,11] and Simon Stael[1,13,*]

[1]Department of Molecular Sciences, Uppsala BioCenter, Swedish University of Agricultural Sciences and Linnean Center for Plant Biology, 75007 Uppsala, Sweden
[2]Department of Functional & Evolutionary Ecology, University of Vienna, Djerassiplatz 1, 1030 Vienna, Austria
[3]Department of Biosciences, University of Milan, Via Giovanni Celoria 26, 20133 Milan, Italy
[4]Institute of Plant Biology and Biotechnology (IBBP), Universität Münster, Schlossplatz 8, 48143 Münster, Germany
[5]Department of Materials Science and Engineering, Uppsala University, 75103 Uppsala, Sweden
[6]Science for Life Laboratory, Uppsala University, 75103 Uppsala, Sweden
[7]Department of Plant Biotechnology and Bioinformatics, Ghent University, 9052 Ghent, Belgium
[8]VIB Center for Plant Systems Biology, 9052 Ghent, Belgium
[9]Photon Systems Instruments, 66424 Drasov, Czech Republic
[10]Department of Biological and Environmental Sciences, University of Gothenburg, 40530 Gothenburg, Sweden
[11]Institute of Biophysics, National Research Council of Italy (CNR), 20133 Milan, Italy
[12]These authors contributed equally
[13]Lead contact
*Correspondence: simon.stael@slu.se
https://doi.org/10.1016/j.cub.2025.04.065

SUMMARY

Plants rely on water and light for photosynthesis, but water droplets on leaves can focus light into high-intensity spots, risking photodamage. Excessive light can impair growth or induce cell death, making it essential for plants to detect and respond to light fluctuations. While Ca^{2+} signaling has been linked to high light (HL) acclimation, the subcellular dynamics remain unclear. Here, we investigate Ca^{2+} responses to HL exposure in *Arabidopsis thaliana*. Using a glass bead to simulate light-focusing by water droplets, a biphasic increase of Ca^{2+} concentration was detected in the chloroplast stroma by the genetically encoded calcium indicator YC3.6 and confirmed using a newly established stroma-localized R-GECO1 (NTRC-R-GECO1). The stromal response was largely independent of light wavelength and unaffected in *phot1 phot2* and *cry1 cry2* mutants. Chemical inhibition of photosynthetic electron transport, microscopy-based Fv/Fm experiments, and measurement of the reactive oxygen species (ROS)-redox balance with roGFP-based reporters and Singlet Oxygen Sensor Green (SOSG) chemical dye suggested that photodamage and singlet oxygen contribute to the stromal Ca^{2+} response. While blue and white light also triggered a Ca^{2+} response in the cytosol and nucleus, pharmacological inhibition with cyclopiazonic acid (CPA) and loss-of-function mutants of the Ca^{2+} transporters BIVALENT CATION TRANSPORTER 2 (BICAT2) and endoplasmic reticulum (ER)-type Ca^{2+}-ATPase (ECA) suggested that the HL response depends on a Ca^{2+} exchange between the ER and chloroplast stroma. The response was primarily light dependent but accelerated by increasing external temperature. This study implicates a novel Ca^{2+}-mediated acclimation mechanism to HL stress, a process of growing relevance in the context of climate change.

INTRODUCTION

Plants require water and light for photosynthesis to support their growth. While the effects of water and light availability on development have been widely studied, recent research explores their more subtle influences. For example, rain droplets bending trichomes trigger calcium signals,[1] and water spray alone induces jasmonic acid production,[2] a hormone crucial for growth and defense, highlighting the ability of plants to perceive and react to physical disturbances caused by water. Other sources of water droplets on the leaf surface can come from morning dew or guttation drops,[3] a watery liquid exuded from hydathode pores at leaf edges. Beyond the physical impact of rain, water droplets on plant surfaces can focus sunlight on specific leaf areas through a lensing effect, influenced by droplet size, shape, distribution, and sunlight angle.[4]

Understanding the effects of these localized spots of intense light exposure could provide valuable insights into plant stress responses, photosynthesis, and the evolution of plant adaptations to fluctuating light conditions.

High light (HL) exposure can be harmful to plant growth when light intensity exceeds the plant's ability to use the energy for CO_2 assimilation or safely dissipate the excess energy, often occurring in combination with biotic and abiotic stresses. Plants acclimate to HL stress through short-term and long-term regulatory mechanisms.[5,6] The dissipation of excess excitation energy as heat, known as non-photochemical quenching, is induced within seconds of HL exposure.[6] A transcriptional response occurs within seconds to minutes as well.[7] Within minutes, the chloroplast avoidance response relocates chloroplasts along the anticlinal sides of the cells.[8] After hours to days, further transcriptional, translational, and post-translational responses lead to an altered composition of the photosynthetic apparatus, anthocyanin biosynthesis, and leaf morphology.[5,9,10] Eventually, photodamaged chloroplasts are removed by autophagy, and often cell death occurs.[11,12]

HL damages mainly photosystem II and leads to the inactivation of electron transport and subsequent oxidative damage of the reaction center proteins, in particular of the D1 subunit.[13] The production of reactive oxygen species (ROS) is an integral part of the HL response, as overexcitation of the photosynthetic electron chain leads to the production of singlet oxygen ($^1O_2$) and superoxide ($O_2^{\cdot-}$) that is rapidly converted to hydrogen peroxide (H_2O_2). The higher stability of H_2O_2 makes it the most suitable second messenger of HL stress,[14–16] but the highly reactive $^1O_2$ is also implicated in HL acclimation.[17,18] A myriad of second messengers interact and converge on retrograde signaling from the chloroplast to the nucleus for the plant to acclimate to HL stress.[5]

Unlike ROS, the role of calcium ion (Ca^{2+}) signaling in the HL response remains largely unexplored. Ca^{2+} ions play essential metabolic and structural roles in chloroplasts—for example, in the regulation of photosynthesis and as a component of the oxygen-evolving complex.[19,20] Elevated Ca^{2+} concentrations in the chloroplast stroma ($[Ca^{2+}]_{str}$) were observed in response to a range of stimuli,[21–24] including when plants are transferred from light to darkness.[25–27] Several transporters and channels have been reported to mediate Ca^{2+} signaling in the chloroplast: CHLOROPLAST-LOCALIZED MITOCHONDRIAL CALCIUM UNIPORTER (cMCU),[24] the non-selective BIVALENT CATION TRANSPORTER 1/CA^{2+}/H^+ ANTIPORTER1/PHOTOSYNTHESIS AFFECTED MUTANT71 (BICAT1/CCHA1/PAM71),[26,28,29] BIVALENT CATION TRANSPORTER 2/CALCIUM/MANGANESE CATION TRANSPORTER 1 (BICAT2/CMT1),[26,30] and the two POLLUX-like proteins PLASTID ENVELOPE ION CHANNELS 1 and 2 (PEC1/2), although it is unclear if PEC1 and PEC2 are permeable to Ca^{2+} or work in concert with yet unknown Ca^{2+}-permeable channels.[31] However, none of these channels and transporters have been linked to HL acclimation. Potential Ca^{2+}-binding proteins have been identified in chloroplasts.[32] Notably, CALCIUM SENSING RECEPTOR (CAS), a thylakoid-membrane-localized Ca^{2+}-binding protein that is phosphorylated in an HL- and Ca^{2+}-dependent manner, is required for efficient HL acclimation in *Arabidopsis thaliana* (hereafter *Arabidopsis*).[33–35] In the single-cell green alga *Chlamydomonas reinhardtii* (hereafter *Chlamydomonas*), CAS regulates the expression of photoprotective genes, and loss-of-function lines are sensitive to HL.[36] Calredoxin, a protein that combines four Ca^{2+}-binding EF-hands with a redox-regulatory thioredoxin, was linked to antioxidant defense and HL stress in *Chlamydomonas* but is not conserved in plants.[37,38] These reports implicate a potential role for $[Ca^{2+}]_{str}$ dynamics in HL acclimation.

Ca^{2+} dynamics can be visualized using genetically encoded calcium indicators (GECIs). However, GECIs require light as in- and/or output (fluorescence and chemiluminescence), complicating the use of external sources of light. Likely owing to these difficulties, the potential existence, dynamics, mechanism of induction, and origin of HL-induced $[Ca^{2+}]_{str}$ have remained obscure for long and were only recently observed in *Chlamydomonas* and the diatom *Phaeodactylum tricornutum* (hereafter *Phaeodactylum*).[39,40]

We report here the discovery of an HL-induced Ca^{2+} response in *Arabidopsis*. To investigate this phenomenon, we used high-intensity lasers and white light sources to replicate the water droplet lensing effect, allowing precise control and spatiotemporal resolution in tracking Ca^{2+} dynamics.

RESULTS

Blue light elicits a biphasic Ca^{2+} response in chloroplasts

We attempted to elicit a $[Ca^{2+}]_{str}$ response in cotyledons expressing a chloroplast-targeted GECI, 2BAM4-YC3.6,[41] with 100% of transmitted microscopy light. When this approach failed, we drew inspiration from how water droplets focus light (Figures 1A and 1B). Indeed, focusing light through a glass bead triggered a $[Ca^{2+}]_{str}$ response (Figures 1C and 1D). We ruled out a potential touch stimulus, which is known to trigger Ca^{2+} signaling, by intermittent imaging in the absence of transmitted light illumination (Figure S1A).

Historically, light-to-dark-induced $[Ca^{2+}]_{str}$ was measured with luminescent Ca^{2+} sensors such as aequorin.[25] Attempting to confirm a dark-induced $[Ca^{2+}]_{str}$ increase, we realized that the blue excitation light (436 ± 20 nm wavelength) required for imaging 2BAM4-YC3.6 triggered a $[Ca^{2+}]_{str}$ increase, dependent on the imaging time: taking images of 300 ms duration every 60 s had no effect, but a 5-s interval triggered a $[Ca^{2+}]_{str}$ increase (Figure S1B). A 90 s pulse of blue light was sufficient to trigger the $[Ca^{2+}]_{str}$ response (Figure S1C). Changing the imaging frequency should not affect the Ca^{2+} signal. Together with the observation that focused light triggered a $[Ca^{2+}]_{str}$ increase (Figures 1C and 1D), we set out to analyze this intriguing response in more detail.

To confirm that blue light exposure triggers the $[Ca^{2+}]_{str}$ increase, 2BAM4-YC3.6 signals were measured in cotyledons, leaves, and roots with a blue laser (405 nm). In cotyledons, switching from quasi-darkness (intermittent imaging) to continuous illumination triggered a fast $[Ca^{2+}]_{str}$ spike that lasted for about 30 s and returned to a basal level before rising again more slowly and persistently (Figures 2A, S1D, and S1E; Video S1). The fast $[Ca^{2+}]_{str}$ spike arose from a handful of random chloroplasts in the images (indicated in Figure 2C at 8, 16, and 40 s), while the later persistent $[Ca^{2+}]_{str}$ increase occurred in almost all chloroplasts (Figure 2C at 650 s). Interestingly, mesophyll

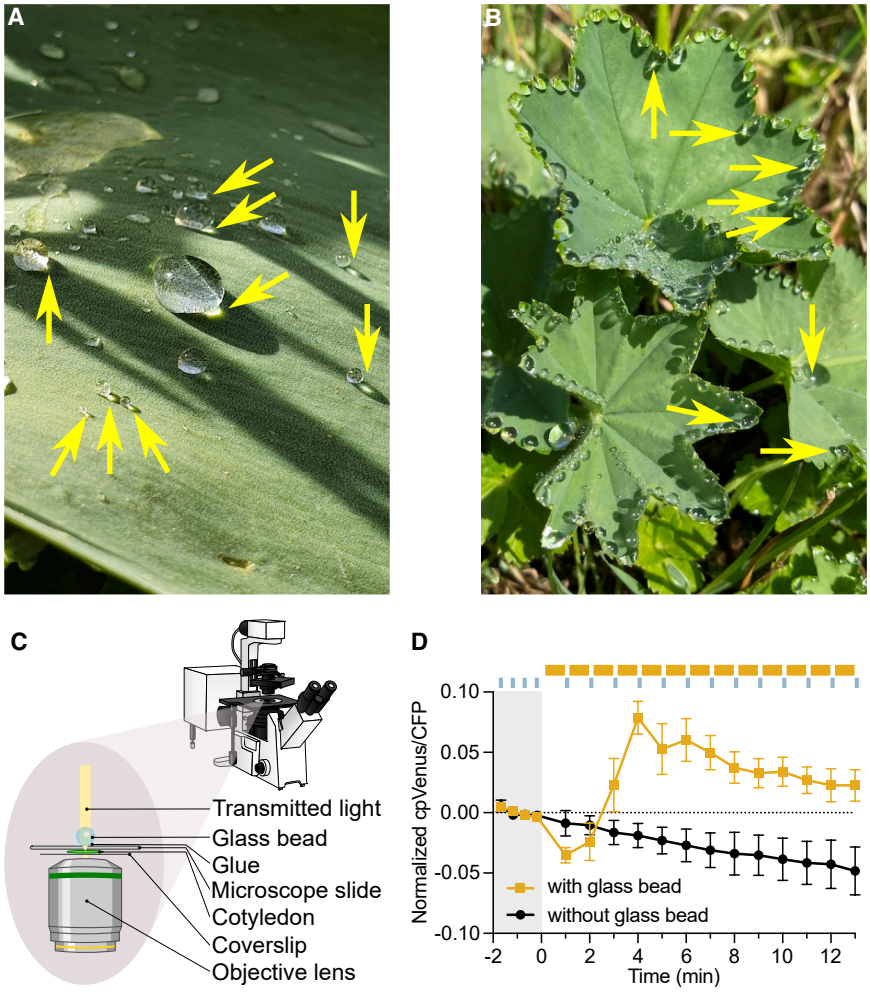

Figure 1. Exposure of plants to focused light triggers $[Ca^{2+}]_{str}$ dynamics

(A) Pictures of water drops on tulip leaves (*Tulipa* × *gesneriana*) outside in the sun after a rain shower.

(B) Guttation drops at the leaf edge of Lady's Mantle (*Alchemilla sp.*). Sunlight is focused through the water drops and projected on the leaf surface (indicated with yellow arrows in A and B).

(C) Diagram of the glass bead setup that was used to mimic the focus effect of water drops, on a confocal microscope. Transmitted light is focused through a glass bead glued to the microscope slide. Confocal-scanning-laser-microscope (CSLM) icon by Database Center for Life Science (DBCLS) https://togotv.dbcls.jp/en/pics.html licensed under CC-BY 4.0.

(D) $[Ca^{2+}]_{str}$ dynamics induced by focused white halogen light (with glass bead, $n = 8$) and by non-focused white halogen light (without glass bead, $n = 5$) in cotyledons of the 2BAM4-YC3.6 expressing *Arabidopsis* line. Light treatment is indicated with a yellow bar. Cotyledons were intermittently imaged every 1 min between the white light stimuli. Curves represent mean ± SEM.

See also Figure S1.

chloroplasts had a delayed response compared with the smaller and scattered epidermal chloroplasts[42] (Figures 2B and 2C). Guard cell chloroplasts were even more delayed in their response (Figure 2B). True leaves behaved similarly to cotyledons (Figure S1F). Neither the fast spike nor later persistent $[Ca^{2+}]_{str}$ increase occurred in roots (Figure 2A), indicating that only photosynthetically active plastids (chloroplasts) respond to blue light exposure.

A newly established, red-shifted, and chloroplast-localized GECI, NTRC-R-GECO1, confirms the blue light-induced stromal Ca^{2+} response

For greater flexibility, parallel imaging of multiple GECIs, and more robust analyses, we targeted a red-shifted GECI, R-GECO1,[43] to the chloroplast stroma using the nicotinamide adenine dinucleotide phosphate (NADPH) thioredoxin reductase C targeting peptide (NTRC-R-GECO1; Figures S1G, S2A, and S2B). Selected lines grew similar to wild type (Figure S2C), and the NTRC-R-GECO1 signal overlapped with chlorophyll autofluorescence (Figure S2D). NTRC-R-GECO1 allows imaging of the $[Ca^{2+}]_{str}$ response at a different wavelength (561 nm) than the blue light stimulus (405 nm). Under continuous blue light, the fast $[Ca^{2+}]_{str}$ spike rose as quickly but declined more slowly (Figure 2D; Video S2), while the persistent $[Ca^{2+}]_{str}$ increase behaved similarly to the 2BAM4-YC3.6 experiment.

Additionally, we produced a mitochondria-targeted R-GECO1, making use of the mitochondria-localized 2-oxoglutarate dehydrogenase E1 targeting peptide (AKDE1-R-GECO1; Figure S2). The selected lines accumulated similar amounts of R-GECO1 protein compared with NTRC-R-GECO1, and a previously established cyto/nuclear R-GECO1 line did not show obvious growth phenotypes, and AKDE1-R-GECO1 signal overlapped with a mitochondrial dye in protoplasts (Figures S2C–S2E). The $[Ca^{2+}]$ dynamics of the mitochondria did not respond to a blue light stimulus (Figure S2F). On the contrary, the AKDE1-R-GECO1 signal decreased, possibly due to bleaching of the fluorophore, suggesting similar bleaching may occur for NTRC-R-GECO1.

The fast $[Ca^{2+}]_{str}$ spike occurred when imaged only with a 561 nm laser (the higher value compared with those in Figure 2D is due to normalization), but the later persistent $[Ca^{2+}]_{str}$ increase was missing (Figure S1H). R-GECO1 is known to be pH sensitive.[44] Therefore, we estimated stromal pH changes with a circularly permuted yellow fluorescent protein (cpYFP).[45] Upon blue light exposure, the stromal pH behaved similar to the fast $[Ca^{2+}]_{str}$ spike, which is likely explained by a pH effect on the NTRC-R-GECO1 sensor (Figure S1I). All chloroplasts had an average signal increase, reflecting light-induced stromal alkalinization,[46] but only few chloroplasts experienced a $[Ca^{2+}]_{str}$ spike (Figures S1J and S1K). The persistent increase of NTRC-R-GECO1 signal was exclusively due to $[Ca^{2+}]_{str}$ and root plastids did not respond to blue light exposure (Figures 2A and 2D). Epidermal and mesophyll chloroplasts also displayed

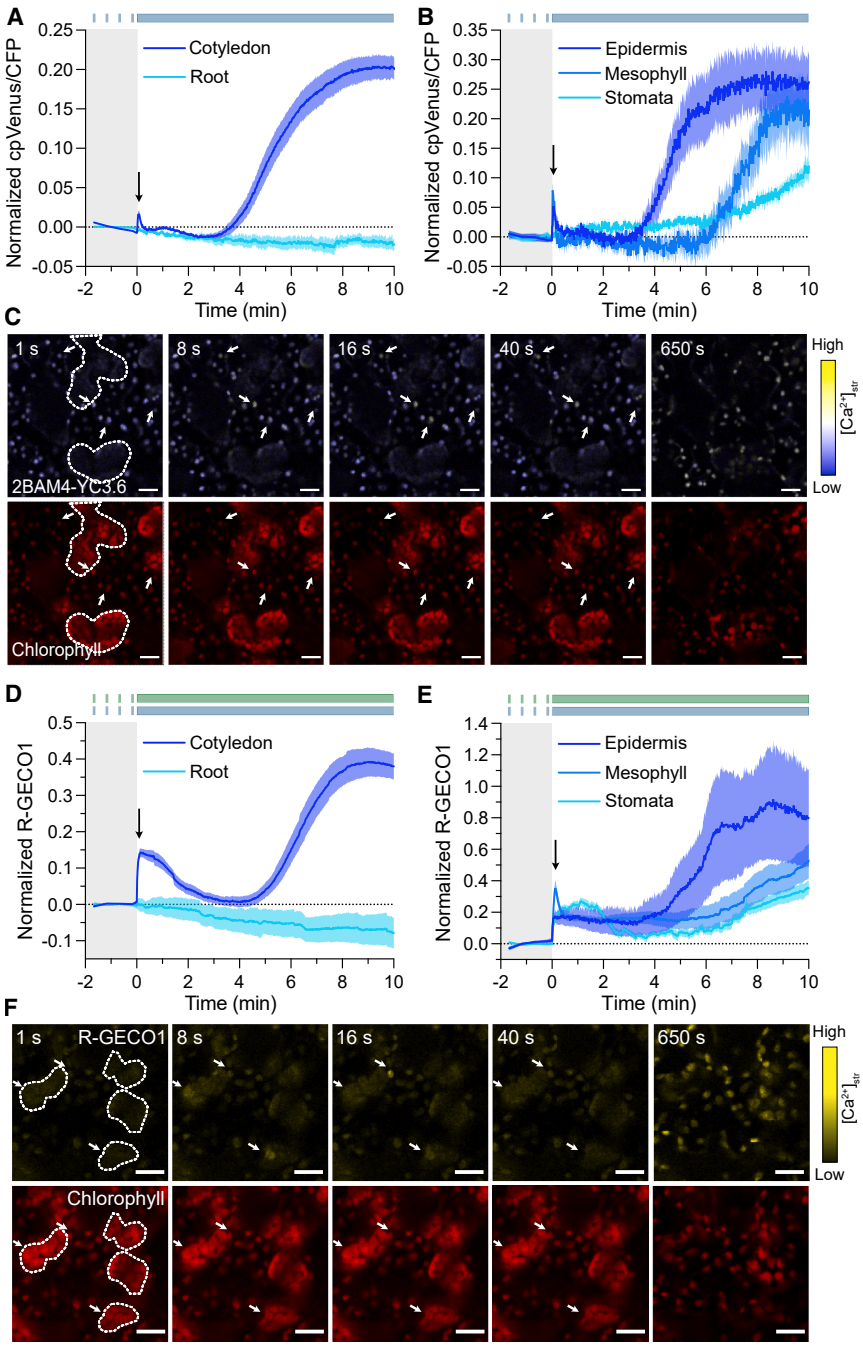

Figure 2. Blue light induces biphasic $[Ca^{2+}]_{str}$ dynamics in chloroplasts

(A) $[Ca^{2+}]_{str}$ dynamics induced by a 10% 405 nm laser in cotyledons and roots of 2BAM4-YC3.6 line. $n = 6$. The black arrow indicates the initial fast spike of $[Ca^{2+}]_{str}$. The blue bar indicates the light regime switching from intermittent imaging (baseline) to continuous imaging (blue light stimulus). Curves represent mean ± SEM.

(B) Epidermis ($n = 5$), mesophyll ($n = 6$), and stomata ($n = 12$) cells of 2BAM4-YC3.6 expressing cotyledons show a heterogeneous response in $[Ca^{2+}]_{str}$ dynamics induced by a 10% 405 nm laser. Curves represent mean ± SEM.

(C) Merged cpVenus and CFP signals (top) and chlorophyll (bottom) of the 2BAM4-YC3.6 expressing line. Scale bar, 20 μm.

(D) $[Ca^{2+}]_{str}$ dynamics induced by a 10% 405 nm laser in cotyledons and roots of NTRC-R-GECO1 line. NTRC-R-GECO1 was additionally excited by a 1% 561 nm laser (green bar). $n = 5$. Curves represent mean ± SEM.

(E) Epidermis ($n = 6$), mesophyll ($n = 15$), and stomata ($n = 15$) cells of cotyledons expressing NTRC-R-GECO1 show heterogeneous $[Ca^{2+}]_{str}$ kinetics induced by a 10% 405 nm laser. Curves represent mean ± SEM.

(F) R-GECO1 signal (top) and chlorophyll (bottom) of NTRC-R-GECO1 line. Scale bar, 50 μm. White arrows in 1, 8, 16, and 40 s indicate chloroplasts with increased signal, and white dashed lines indicate chloroplasts of mesophyll cells in (C) and (F).

See also Figures S1–S3 and Videos S1, S2, and S3.

different kinetics of persistent $[Ca^{2+}]_{str}$ elevations, while the signatures of mesophyll and guard cell chloroplasts were quite similar (Figure 2E). The fast $[Ca^{2+}]_{str}$ spike occurred in seemingly random chloroplasts irrespective of tissue localization (Figure 2F). In conclusion, the NTRC-R-GECO1 experiments recapitulated the 2BAM4-YC3.6 data, while visualization was clearer, likely due to NTRC-R-GECO1's higher, more uniform expression and greater dynamic range.

Finally, using a new setup for imaging soil-grown plants by confocal microscopy, we characterized the blue light-induced $[Ca^{2+}]_{str}$ response in non-detached leaves (Figures S3A and S3B; Video S3). Intermittent 561 nm imaging did not affect the $[Ca^{2+}]_{str}$ response, while continuous exposure increased the NTRC-R-GECO1 signal (Figures S3C and S3D), likely because of stromal alkalinization. Concomitant exposure to a 405 nm laser produced a similar persistent $[Ca^{2+}]_{str}$ increase to detached cotyledons, albeit with a faster dynamic (Figures S3E and S3F). This could be due to the slightly stronger light stimulus (Table S1) or an inherent feature of non-detached mature leaves. Cotyledons and first true leaves were imaged from the abaxial side. Non-detached leaves were imaged from the adaxial side. Hence, chloroplasts on both sides of the leaf reacted similarly to the blue light stimulus. Taken together, these data show that the blue light-induced $[Ca^{2+}]_{str}$ response occurs in chloroplasts from cotyledons, first true leaves, and mature non-detached leaves.

The stromal Ca^{2+} response is proportional to the light intensity

To determine whether light intensity alters the $[Ca^{2+}]_{str}$ response, we varied the strength of the 405 nm laser. Laser power was

measured at the focal point on the microscope and was within or exceeded the range generally considered to be HL, e.g., >1,000 μmol photons m^{-2} s^{-1} (Table S1). 5% laser power triggered the fast $[Ca^{2+}]_{str}$ spike; however, the persistent $[Ca^{2+}]_{str}$ increase was absent (Figure 3A). Increasing the intensity of blue light to 7.5%, 10%, and 20% triggered stronger fast $[Ca^{2+}]_{str}$ spikes, and now also the persistent $[Ca^{2+}]_{str}$ elevations were observed (Figures 3A and 3B). While the amplitudes of the persistent $[Ca^{2+}]_{str}$ elevations remained similar, the time to reach maximum (TRM) of the persistent $[Ca^{2+}]_{str}$ increase was significantly shortened with increased light intensity, and the area under the curve (AUC) increased with the light intensity (Figures 3C and 3D), implicating a larger $[Ca^{2+}]_{str}$ accumulation upon higher light intensities during this period of time. The TRM of 5% blue light had heterogeneous maximum values and therefore was not included in Figures 3C and 3G. Taken together, the persistent $[Ca^{2+}]_{str}$ increase required HL intensities, and its kinetics correlated with laser strength.

Red and white light trigger similar stromal Ca^{2+} responses as blue light

Next, we tested whether the Ca^{2+} response was blue light-specific or triggered by other wavelengths. In combination with a 5% 405 nm laser, required for imaging 2BAM4-YC3.6 but insufficient to trigger persistent $[Ca^{2+}]_{str}$ elevations, red light (633 nm) induced a similar Ca^{2+} response as blue light (Figure 3E). The AUC for the fast $[Ca^{2+}]_{str}$ spike was unaltered by different light intensities (Figure 3F), although the amplitude slightly increased, similar to the blue light response. For the persistent $[Ca^{2+}]_{str}$ increase, higher 633 nm laser strength led to a shorter TRM and a larger AUC (Figures 3G and 3H). Red light required higher laser strength than blue light to elicit a comparable persistent $[Ca^{2+}]_{str}$ increase at equal power (W) (Figure 3; Table S1).

Natural light conditions were mimicked by white light, but in contrast to the transmitted light used previously (Figure 1D), a persistent $[Ca^{2+}]_{str}$ increase could be induced using a mercury short-arc lamp that uses a high-pressure xenon plasma operating at 120 volts (HXP 120 V) without focusing the light through a glass bead (Figures 3I–3K). Additionally, a halogen light source also triggered a persistent $[Ca^{2+}]_{str}$ increase (Figures S4A–S4C). Unfortunately, the fast $[Ca^{2+}]_{str}$ spike could not be observed with these imaging settings. Similar to blue light (Figure S1B), the duration of white light exposure determined the $[Ca^{2+}]_{str}$ dynamic. The amplitude was higher after 5 min of light exposure compared with 1.5 min and remained constant thereafter. Continuous white light led to a subsequent decrease of $[Ca^{2+}]_{str}$ (Figure S4A), similar to the $[Ca^{2+}]_{str}$ dynamic of 20% blue light (Figure 3A). Not all white light intensities triggered a $[Ca^{2+}]_{str}$ response. For example, using an on-stage illumination system that delivers white light from a light-emitting diode (LED) to the microscope slide,[46] no $[Ca^{2+}]_{str}$ responses occurred upon switching from 40 μmol photons m^{-2} s^{-1} white light to 600 or 1,100 photons μmol m^{-2} s^{-1} (Figure S5). Altogether, our results indicate that a similar perception mechanism exists for HL intensities of either blue, red, or white light, triggering highly similar $[Ca^{2+}]_{str}$ dynamics, but a certain threshold of HL intensity is required to trigger the response.

The HL-induced stromal Ca^{2+} response coincides with ROS production

Since HL induces photosynthesis-derived ROS,[15] we monitored cytosolic and stromal ROS using a fusion protein of the redox-sensitive variant of green fluorescent protein with the yeast oxidant receptor peroxidase 1 (roGFP2-Orp1),[47] a genetically encoded sensor specific for H_2O_2 as an oxidant and the glutathione system as reductant.[48,49] Blue light triggered a pronounced H_2O_2 accumulation in the cytosol and chloroplast stroma (Figure 4A). Similar responses were recorded with the genetically encoded glutathione redox potential sensor, TKTP-glutaredoxin 1(GRX1)-roGFP2 (Figure S6A), and a TKTP-GRX1-roGFP2 × NTRC-R-GECO1 crossed line, ascertaining that redox and $[Ca^{2+}]_{str}$ changes occurred in the same chloroplasts (Figures S6B–S6D). The fast $[Ca^{2+}]_{str}$ spike preceded stromal H_2O_2 accumulation, while the persistent $[Ca^{2+}]_{str}$ increase occurred almost 2 min later. The cytosol accumulated H_2O_2, as previously reported,[15] albeit slower than in the stroma. Interestingly, 10% blue light triggered a strong stromal H_2O_2 accumulation but a much weaker and delayed $[Ca^{2+}]_{str}$ increase (Figure 4B), suggesting a disconnect between H_2O_2 accumulation and the $[Ca^{2+}]_{str}$ response.

The HL regimes were quenching chlorophyll autofluorescence (Figure 4C), which is indicative of enhanced non-photochemical quenching[6] or damage to the photosystems.[12] Therefore, we imaged photosystem II quantum yield (QY) together with $[Ca^{2+}]_{str}$ elevations using a fluorescence kinetic microscope (FKM) from Photon Systems Instruments (PSI) and observed a significant Fv/Fm decrease following a blue light-induced $[Ca^{2+}]_{str}$ increase (Figures S7A–S7C). Imaging with 30% 523 nm light did not induce a typical $[Ca^{2+}]_{str}$ response or drop of Fv/Fm ratio (Figures S7D and S7E), while the increased R-GECO1 signal likely resulted from stromal alkalinization, as previously observed (Figures S1H and S1I). These results indicate that our HL treatment directly impacts the maximum QY of PSII.

To confirm the involvement of the photosynthetic electron transport reactions in the $[Ca^{2+}]_{str}$ response, we tested the effect of 3-(3,4-dichlorophenyl)-1,1-dimethylurea (DCMU), which irreversibly blocks the Q_B plastoquinone binding site of photosystem II, obstructing the electron flow from photosystem II to plastoquinone. DCMU experiments were performed using protoplasts, as penetrance of chemicals is more effective, as shown, for example, with the mitochondrial dye (Figure S2D). White light-induced persistent $[Ca^{2+}]_{str}$ increase reached a maximum earlier in DCMU-treated protoplasts (Figure 4D), while the amplitude remained unaffected. Interestingly, the pH-dependent increase of the R-GECO1 signal was abolished, indicating that, as expected,[15] light-induced stromal alkalinization was inhibited by DCMU treatment. Dibromothymoquinone (DBMIB), a plastoquinone analog and alternative inhibitor that blocks binding at the Q_o-site of the Cyt b_6f complex, also led to an earlier $[Ca^{2+}]_{str}$ accumulation, albeit to a lesser extent than DCMU (Figure 4E). Treatment with methyl viologen (MV), which leads to superoxide ($O_2^{\cdot-}$) production by funneling electrons from photosystem I to oxygen (O_2), did not markedly alter the $[Ca^{2+}]_{str}$ response (Figure 4F).

As stromal H_2O_2 accumulation and $[Ca^{2+}]_{str}$ increase were disconnected at lower light intensity (Figure 4B), and DCMU treatment accelerated the stromal Ca^{2+} response, we tested

CellPress
OPEN ACCESS

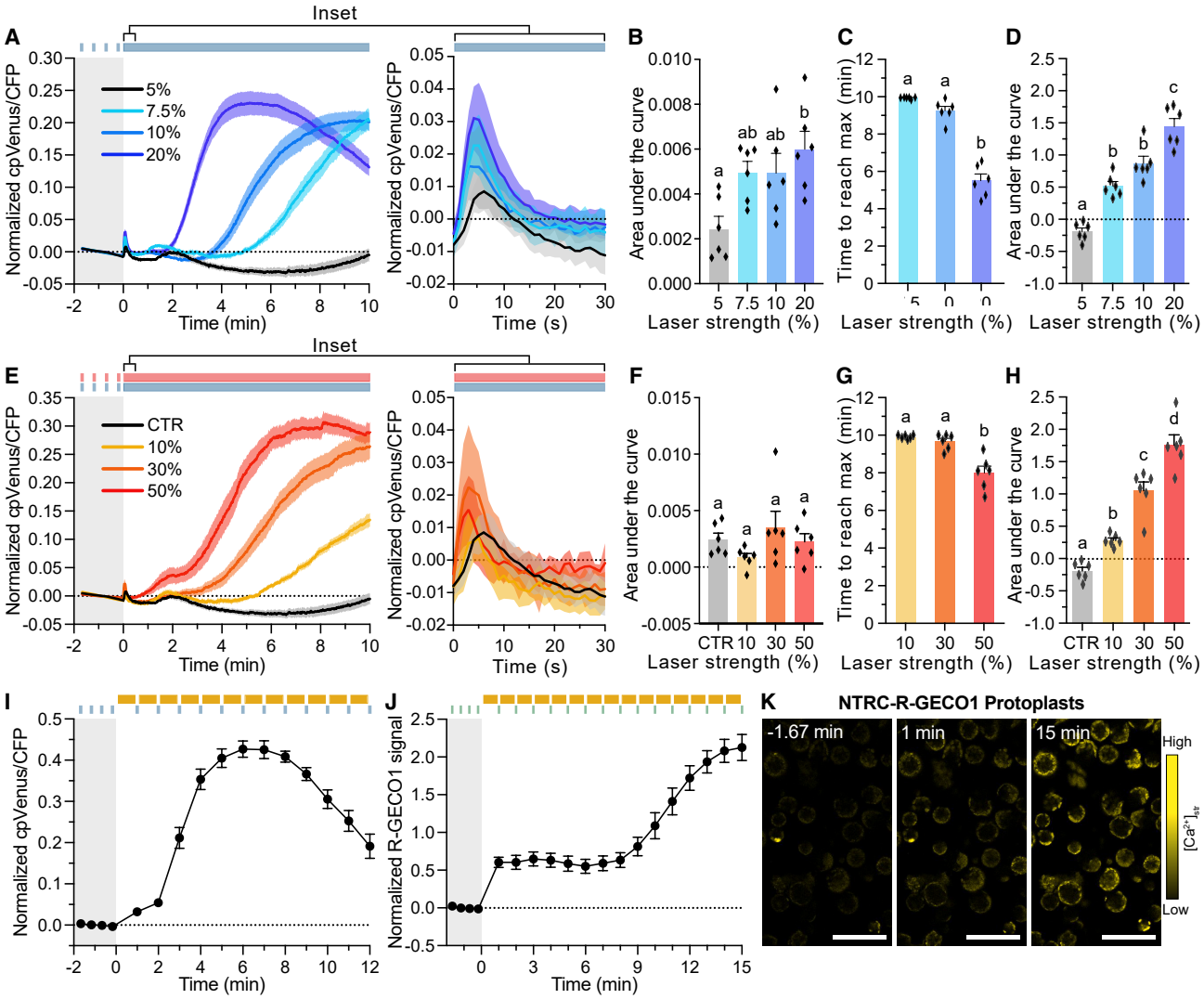

Figure 3. Different light intensities and qualities induce different $[Ca^{2+}]_{str}$ signals

(A) $[Ca^{2+}]_{str}$ dynamics induced by 5% (56 μW), 7.5% (86 μW), 10% (113 μW), and 20% (235 μW) 405 nm laser (blue bar) in cotyledons of the 2BAM4-YC3.6 expressing line. $n = 6$. The fast $[Ca^{2+}]_{str}$ spike in the initial 30 s of HL stimulus is shown in the inset. Curves represent mean ± SEM.

(B and F) Areas under the curves of the fast $[Ca^{2+}]_{str}$ spike in the initial 30 s of HL stimulus. $n = 6$. Different letters above the bars indicate significant differences (one-way ANOVA, $p \leq 0.05$). Error bars indicate SEM.

(C and G) TRM values of the persistent $[Ca^{2+}]_{str}$ increase in the 10 min of HL stimulus. $n = 6$. Different letters above the bars indicate significant differences (one-way ANOVA, $p \leq 0.05$). Error bars indicate SEM.

(D and H) Areas under the curves of the persistent $[Ca^{2+}]_{str}$ increase in the 10 min of HL stimulus. $n = 6$. Different letters above the bars indicate significant differences (one-way ANOVA, $p \leq 0.05$). Error bars indicate SEM.

(E) $[Ca^{2+}]_{str}$ dynamics induced by 5% (56 μW) 405 nm laser with additional 0% (control; CTR), 10% (59 μW), 30% (180 μW), and 50% (310 μW) 633 nm laser (red bar) in cotyledons of the 2BAM4-YC3.6 line. CTR and 5% 405 nm laser in (A) are the same data used for comparison. $n = 6$. Curves represent mean ± SEM.

(I) $[Ca^{2+}]_{str}$ dynamics induced by white light (yellow bars) in 2BAM4-YC3.6 line. Cotyledons were intermittently imaged (blue bars) between the white light stimuli. $n = 6$. Curves represent mean ± SEM.

(J) $[Ca^{2+}]_{str}$ dynamics induced by white light in protoplasts of NTRC-R-GECO1 line. $n = 11$. Curves represent mean ± SEM.

(K) R-GECO1 signals of protoplasts of NTRC-R-GECO1 line, at the time points of 1.67 min before, 1 min after, or 15 min after white light stimuli. Scale bar, 100 μm. See also Table S1 and Figures S4 and S5.

the potential involvement of other photosynthetically derived ROS. DCMU prevents the reduction of plastoquinone[50]; hence, if ROS were involved in the HL-induced $[Ca^{2+}]_{str}$ response, they would likely be generated early during photosynthetic electron transport, such as $^1O_2$ at photosystem II.[51] Indeed, HL triggered a consistent $^1O_2$ increase in chloroplasts from NTRC-R-GECO1 protoplasts stained with Singlet Oxygen Sensor Green (SOSG) (Figures 4G and 4H), and SOSG did not interfere with the HL-induced Ca^{2+} response (Figures S6E and S6F). Taken together, the persistent $[Ca^{2+}]_{str}$ increase is likely caused by photoinhibition-derived ROS, especially $^1O_2$.

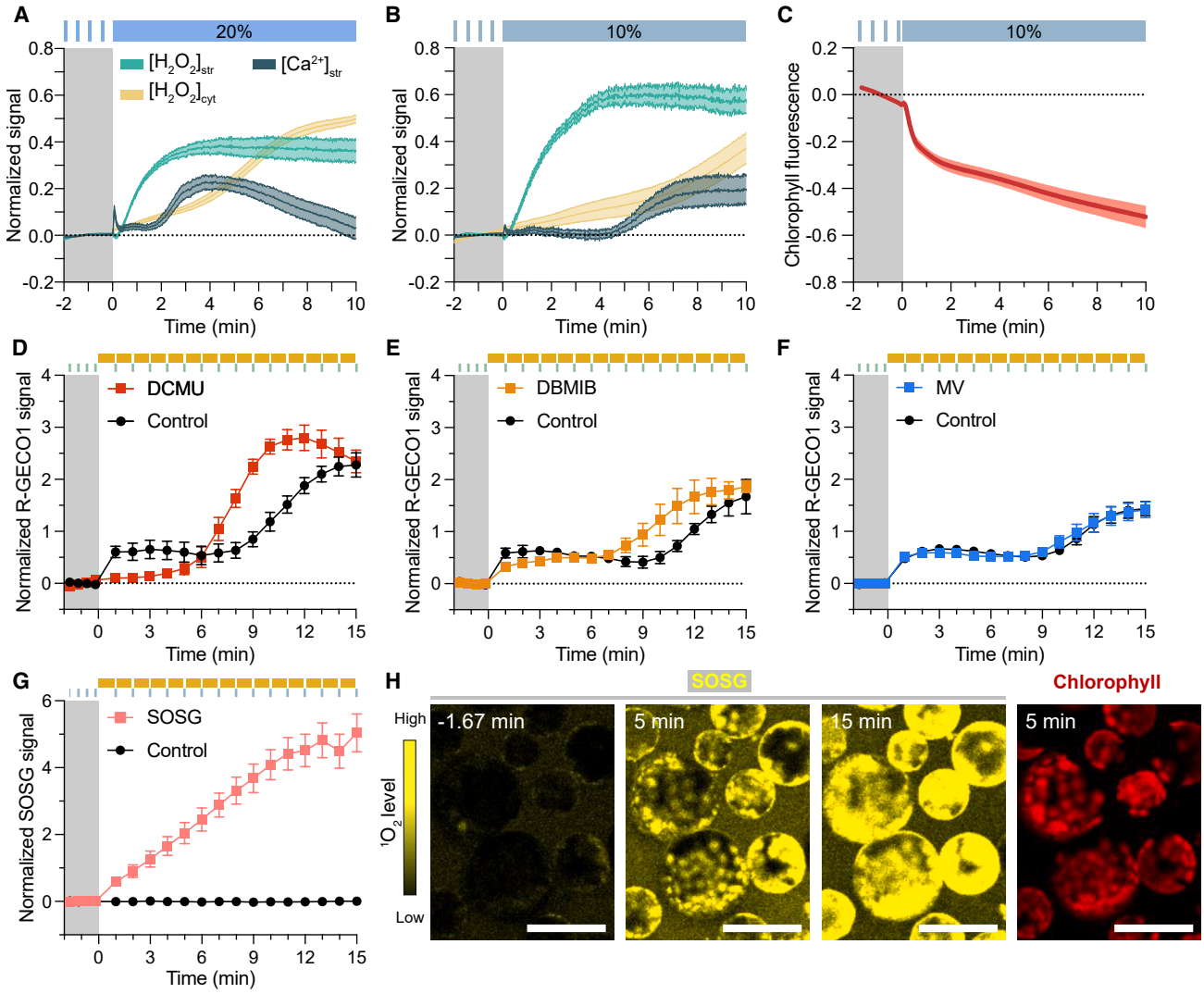

Figure 4. HL-induced $[Ca^{2+}]_{str}$ dynamics interact with ROS and photosynthesis

(A) $[H_2O_2]_{str}$, $[H_2O_2]_{cyt}$, and $[Ca^{2+}]_{str}$ induced by 20% 405 nm laser light (blue bar) in cotyledons of TKTP-roGFP2-Orp1, cyto-roGFP2-Orp1, and 2BAM4-YC3.6 lines. $n = 5$. Curves represent mean ± SEM.

(B) $[H_2O_2]_{str}$, $[H_2O_2]_{cyt}$, and $[Ca^{2+}]_{str}$ induced by a 10% 405 nm laser (blue bar). $n = 5$. Curves represent mean ± SEM.

(C) Chlorophyll fluorescence intensity under 10% 405 nm laser (blue bar). $n = 7$. Curves represent mean ± SEM.

(D) $[Ca^{2+}]_{str}$ dynamics induced by white light (yellow bars) in protoplasts of NTRC-R-GECO1-expressing plants. Protoplasts were pre-treated with 10 μM DCMU ($n = 5$) or 0.1% DMSO (control, $n = 6$). Curves represent mean ± SEM.

(E) $[Ca^{2+}]_{str}$ dynamics of NTRC-R-GECO1 line. Protoplasts were pre-treated with 10 μM DBMIB ($n = 7$) or 0.1% ethanol (control, $n = 3$). Curves represent mean ± SEM.

(F) $[Ca^{2+}]_{str}$ dynamics of NTRC-R-GECO1 line. Protoplasts were pre-treated with 50 μM MV ($n = 5$) or control ($n = 5$). Curves represent mean ± SEM.

(G) $[^1O_2]$ induced by white light in protoplasts of Col-0. Protoplasts were pre-treated with 100 μM $^1O_2$ dye SOSG ($n = 15$) or 1% methanol (control, $n = 3$). Curves represent mean ± SEM.

(H) SOSG signal and chlorophyll fluorescence in protoplasts of Col-0. Scale bar, 50 μm.

See also Figures S6 and S7.

Stromal Ca^{2+} elevations are caused by light rather than a temperature component of HL

Previously, heat shock was found to induce $[Ca^{2+}]_{str}$ elevations.[52] To distinguish whether the HL-induced $[Ca^{2+}]_{str}$ response is caused by light absorption or a temperature effect, we conducted HL experiments under different temperature regimes. At 40°C, the initial $[Ca^{2+}]_{str}$ level was elevated, likely because of heat shock, as previously observed by Lenzoni and Knight[52] (Figure 5A). However, $[Ca^{2+}]_{str}$ dropped upon continuous HL treatment and increased afterward. Non-normalized data illustrate the difference between the initial $[Ca^{2+}]_{str}$ at 40°C and those at lower temperatures. Temperature interfered with the response, as $[Ca^{2+}]_{str}$ rose faster along with the temperature increase, albeit not to the extent observed at 40°C.

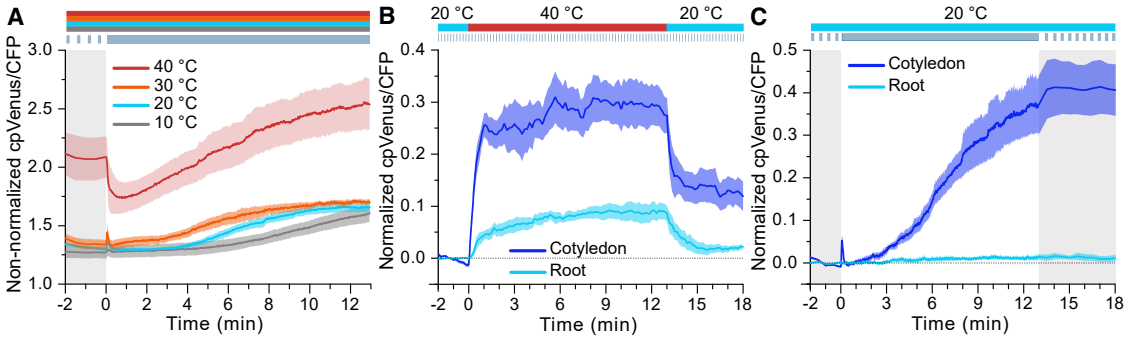

Figure 5. HL-induced $[Ca^{2+}]_{str}$ dynamics are influenced by temperature

(A) $[Ca^{2+}]_{str}$ dynamics induced by a 10% 405 nm laser (dark blue bar) in cotyledons of the 2BAM4-YC3.6 expressing plants at 10°C (gray bar), 20°C (light blue bar), 30°C (orange bar), and 40°C (red bar). $n = 5$. Curves represent mean ± SEM.

(B) $[Ca^{2+}]_{str}$ dynamics of 2BAM4-YC3.6 expressing cotyledons/roots under a temperature shift (20°C to 40°C to 20°C). $n = 5$. Curves represent mean ± SEM.

(C) $[Ca^{2+}]_{str}$ dynamics of 2BAM4-YC3.6 cotyledons/roots under light shift (intermittent imaging to continuous imaging to intermittent imaging) at constant 20°C. $n = 5$. Curves represent mean ± SEM.

See also Figure S8.

Moreover, the $[Ca^{2+}]_{str}$ dynamics looked overall similar to those observed previously without temperature control.

We observed an increase of $[Ca^{2+}]_{str}$ upon heat shock (40°C) in root cells (Figure 5B), while a light intensity that triggers $[Ca^{2+}]_{str}$ in green tissues had no effect on $[Ca^{2+}]_{str}$ in roots (Figure 5C). This indicates that our experimental HL system did not cause a strong temperature effect, at least not in roots. Furthermore, the Ca^{2+} signatures triggered by heat shock and HL in cotyledons differed: the initial $[Ca^{2+}]_{str}$ spike was absent following heat shock, and $[Ca^{2+}]_{str}$ rose more slowly during HL compared with heat shock-induced $[Ca^{2+}]_{str}$ elevations (Figures 5B and 5C). Importantly, $[Ca^{2+}]_{str}$ remained high after switching from HL to darkness under continuous cooling at 20°C (Figure 5C), while the $[Ca^{2+}]_{str}$ levels dropped when switching to 20°C after heat shock (Figure 5B). The same imaging setting of the temperature shift experiment was carried out under constant 20°C, ensuring that the imaging setting itself did not trigger any $[Ca^{2+}]_{str}$ changes (Figures S8A–S8C). Using the temperature-sensitive dye rhodamine B (validated previously for intracellular measurements[53]), we confirmed that the temperature remained stable during imaging under conditions similar to Figure 5C (Figures S8D and S8E). Furthermore, the temperature measured with a thermocouple[54] in the protoplast imaging setup (as in Figure 4) remained stable without external temperature control (Figure S8F). In conclusion, the response is primarily driven by light and not heat shock, with external temperature affecting the speed of the persistent $[Ca^{2+}]_{str}$ increase.

The HL-induced Ca^{2+} response reveals an unexpected interaction between the chloroplast and ER Ca^{2+} pools

Ca^{2+} can be stored in subcellular compartments, such as the apoplast, vacuole, and endoplasmic reticulum (ER). The release to cellular localities with low Ca^{2+} concentration and subsequent active transport back to the stores leads to so-called Ca^{2+} signatures.[19,55] To investigate the origin(s) of the HL-induced $[Ca^{2+}]_{str}$ response, we applied HL treatment to a cytosolic GECI, NES-YC3.6[41] (Figure 6A). Unlike the persistent $[Ca^{2+}]_{str}$ increase, a clear $[Ca^{2+}]_{cyt}$ peak occurred at just 5% laser strength (Figures 6B and 6C). Additionally, the $[Ca^{2+}]_{cyt}$ peak was slower than the fast $[Ca^{2+}]_{str}$ spike and preceded the persistent $[Ca^{2+}]_{str}$ increase by several minutes (Figure 6D). Red light induced a persistent $[Ca^{2+}]_{str}$ increase but no significant $[Ca^{2+}]_{cyt}$ peak (Figure 6E), while white light triggered a clear $[Ca^{2+}]_{cyt}$ peak (Figures S4D and S4E). We crossed the NTRC-R-GECO1 line with a cyto-nuclear-targeted GCaMP3 line[56] and subjected it to HL, confirming the observations made with single chloroplast and cytosol-targeted YC3.6 lines (Figures S9A–S9C). Assuming the HL-induced $[Ca^{2+}]_{str}$ response is not directly linked to a $[Ca^{2+}]_{cyt}$ peak, alternative sources for the $[Ca^{2+}]_{str}$ must be considered.

The ER is one of the major Ca^{2+} stores in plant cells, and close contacts between the ER and chloroplasts were observed previously.[57–59] Hence, we tested a potential involvement of the ER in the HL-induced $[Ca^{2+}]_{str}$ response with an ER-localized GECI, ER-GCaMP6-210.[60] In contrast to the cytosol, the $[Ca^{2+}]_{ER}$ response mirrored the stromal response (Figure 6D): $[Ca^{2+}]_{ER}$ dropped concomitant with the fast $[Ca^{2+}]_{str}$ spike (Figure 6D inset), after which it slowly recovered, to decrease again during the persistent $[Ca^{2+}]_{str}$ increase. The $[Ca^{2+}]_{cyt}$ peak was closely followed by a rise of the $[Ca^{2+}]_{ER}$, suggesting a transfer of cytosolic Ca^{2+} to the ER lumen during blue light exposure. GCaMP6 has dual excitation peaks at 410 and 474 nm, corresponding to Ca^{2+}-independent and Ca^{2+}-dependent emissions, respectively,[61] enabling ratiometric imaging and excluding a potential impact of fluorophore photobleaching on the $[Ca^{2+}]_{ER}$ response (Figures S10A–S10D). The $[Ca^{2+}]_{ER}$ response to red light was similar to blue light, though the increase in $[Ca^{2+}]_{ER}$ was less pronounced (Figure 6E), potentially due to the weaker $[Ca^{2+}]_{cyt}$ response to red light (Figures 6D and 6E). The ER and stromal Ca^{2+} responses behaved similarly in an NTRC-R-GECO1 x ER-GCaMP6-210 crossed reporter line (Figures S9E–S9G).

Further evidence for an interaction between the ER and stromal Ca^{2+} pools came from chemical treatments with cyclopiazonic acid (CPA), an inhibitor of type IIA ER-type Ca^{2+}-ATPases (ECAs)[62] that was shown to deplete $[Ca^{2+}]_{ER}$.[60] CPA treatment greatly enhanced the HL-induced fast $[Ca^{2+}]_{str}$ spike and abolished the persistent $[Ca^{2+}]_{str}$ increase (Figures 6F and 6G).

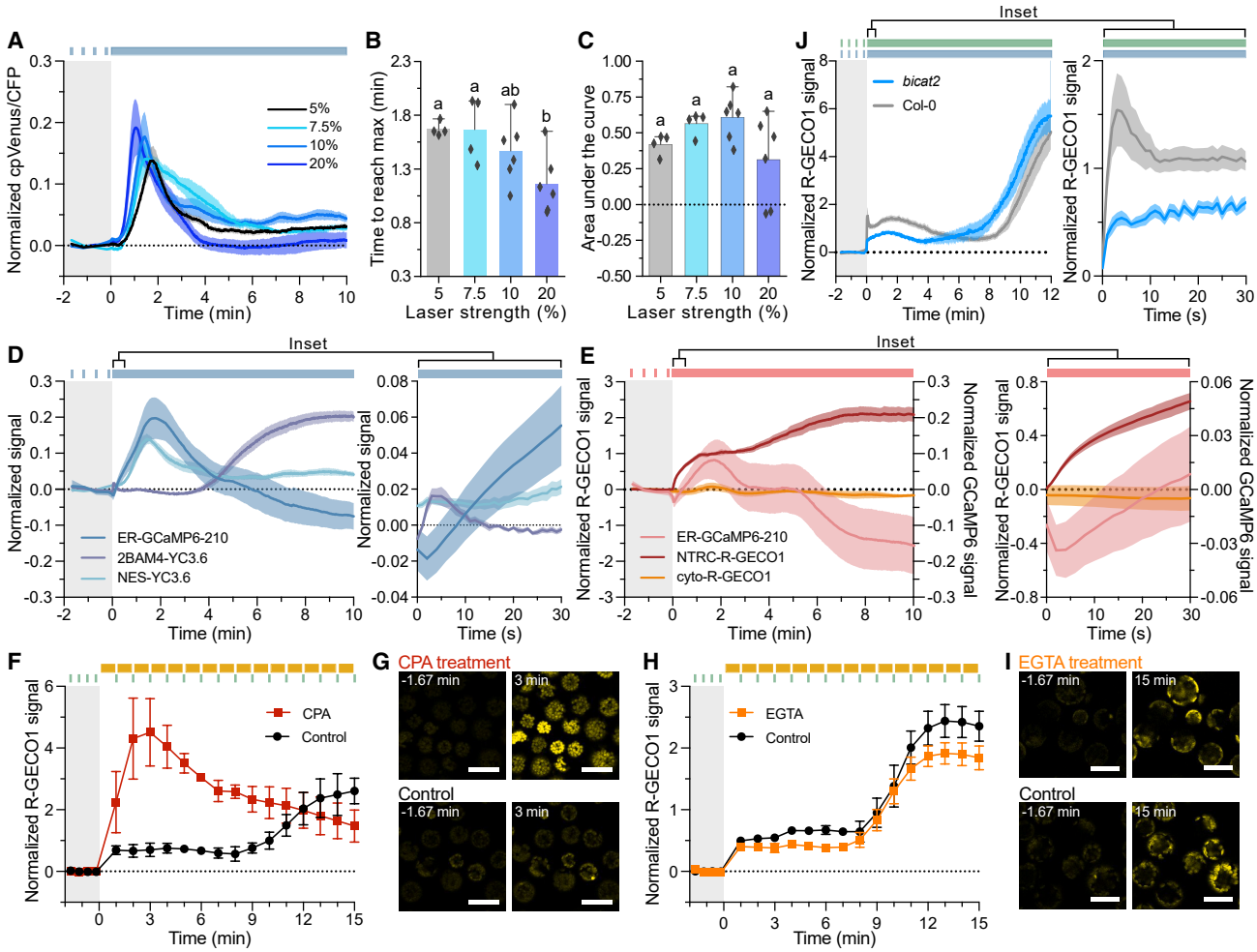

Figure 6. HL-induced $[Ca^{2+}]$ dynamics reveal an interaction between stromal and ER Ca^{2+} pools

(A) $[Ca^{2+}]_{cyt}$ dynamics induced by 5% (56 μW, $n = 4$), 7.5% (86 μW, $n = 4$), 10% (113 μW, $n = 6$), and 20% (235 μW, $n = 6$) 405 nm laser (blue bar) in cotyledons of NES-YC3.6 expressing plants. Curves represent mean ± SEM.

(B) TRM values of $[Ca^{2+}]_{cyt}$ in the 10 min of HL stimulus. Different letters above the bars indicate significant differences (one-way ANOVA, $p \leq 0.05$). Error bars indicate SEM.

(C) Areas under the curves of $[Ca^{2+}]_{cyt}$ in the 10 min of HL stimulus. Different letters above the bars indicate significant differences (one-way ANOVA, $p \leq 0.05$). Error bars indicate SEM.

(D) $[Ca^{2+}]_{str}$ and $[Ca^{2+}]_{cyt}$ induced by a 10% 405 nm laser (blue bar) in cotyledons of 2BAM4-YC3.6 ($n = 6$) and NES-YC3.6 lines ($n = 5$). $[Ca^{2+}]_{ER}$ induced by sequential 10% 405 nm/20% 488 nm laser (blue bar) in cotyledons of ER-GCaMP6-210 line ($n = 6$). $[Ca^{2+}]$ in the initial 30 s of HL stimulus was shown in the inset. Curves represent mean ± SEM.

(E) $[Ca^{2+}]_{ER}$, $[Ca^{2+}]_{str}$, and $[Ca^{2+}]_{cyt}$ induced by 30% 633 nm laser (red bar) in cotyledons of ER-GCaMP6-210 ($n = 7$), NTRC-R-GECO1 ($n = 5$), and cyto-R-GECO1-expressing lines ($n = 5$). Curves represent mean ± SEM.

(F) $[Ca^{2+}]_{str}$ dynamics induced by white light in protoplasts of NTRC-R-GECO1 line. Protoplasts were pre-treated with 25 μM CPA ($n = 4$) or 0.25% DMSO (control, $n = 5$). Curves represent mean ± SEM.

(G) R-GECO1 signals of protoplasts of NTRC-R-GECO1 line under 25 μM CPA treatment or control at the time points of 1.67 min before and 3 min after white light stimuli. Scale bar, 50 μm.

(H) $[Ca^{2+}]_{str}$ dynamics of NTRC-R-GECO1 line. Protoplasts were pre-treated with 10 mM EGTA ($n = 5$) or control ($n = 3$). Curves represent mean ± SEM.

(I) R-GECO1 signals of protoplasts of NTRC-R-GECO1 line under 10 mM EGTA treatment or control at the time points of 1.67 min before and 15 min after white light stimuli. Scale bar, 50 μm.

(J) $[Ca^{2+}]_{str}$ induced by 100% 405 nm laser (blue bar) in *bicat2* and Col-0 protoplasts transiently transformed with pICOz-NTRC-R-GECO1. Data were averaged from 10 protoplasts coming from 3 independent experiments, and background autofluorescence from non-transformed protoplasts was subtracted. Curves represent mean ± SEM.

See also Figures S9–S12 and Videos S4 and S5.

Furthermore, CPA treatment reduced $[Ca^{2+}]_{ER}$ while increasing $[Ca^{2+}]_{str}$ in stomatal guard cells of epidermal peels, regardless of HL exposure (Figures S11A–S11D, S11G, and S11H). The CPA-induced $[Ca^{2+}]_{str}$ increase was independent of a blue light stimulus, as the NTRC-R-GECO1 signal increased with green excitation light only (561 nm; Figures S11E and S11F). Under

blue light conditions that do not trigger an HL response, the CPA-induced $[Ca^{2+}]_{str}$ increase is delayed (Figure S11I), possibly due to the known suppressive effect of light on $[Ca^{2+}]_{str}$ elevation.[25] Importantly, the $[Ca^{2+}]_{cyt}$ response remains stable upon CPA treatment (Figures S11J–S11L), indicating a direct transfer of Ca^{2+} between the ER and chloroplast stroma. Notably, this contrasts with the response in roots, where CPA treatment was previously shown to simultaneously increase $[Ca^{2+}]_{cyt}$ and decrease $[Ca^{2+}]_{ER}$.[60] Chelation of extracellular Ca^{2+} with ethylene glycol-bis(2-aminoethylether)-N,N,N,N-tetraacetic acid (EGTA) had little effect on the persistent $[Ca^{2+}]_{str}$ increase (Figures 6H and 6I). A decrease in amplitude of the persistent $[Ca^{2+}]_{str}$ increase is consistent with the observations by Huang et al.,[63] who observed that extracellular Ca^{2+} chelation with EGTA leads to a 20% reduction in release of $[Ca^{2+}]_{ER}$ to the cytosol.

To explore the genetic basis of the HL-induced Ca^{2+} response, NTRC-R-GECO1 was transiently expressed in protoplasts of loss-of-function mutants for blue light photoreceptors and chloroplast Ca^{2+} transporters and channels, including c*MCU*, *PEC1*, *PEC2*, *BICAT1*, and *BICAT2*.[24,26,31] In plants, blue light is perceived not only by the photosynthetic complexes, where it is absorbed by chlorophyll and carotenoids to drive photosynthesis, but also by photoreceptors like cryptochromes and phototropins. The earlier peak of the persistent $[Ca^{2+}]_{str}$ increase in *phot1-5 phot2-1* and *cry1 cry2* suggests these blue light photoreceptors are not required but may still influence the response, possibly by modulating cytosolic Ca^{2+} signaling (Figures S12A and S12B). The *cmcu* and *pec1 pec2* mutants had a similar response to their respective wild-type controls, although having a slightly lower and higher persistent $[Ca^{2+}]_{str}$ increase, respectively (Figures S12C and S12D). A *bicat1* mutant behaved similarly to wild type (Figure S12E). The *bicat2* and *bicat1 bicat2* mutants were severely impaired in the $[Ca^{2+}]_{str}$ response, with a near complete lack of the fast $[Ca^{2+}]_{str}$ spike in *bicat2* (Figures 6J, S12F, and S12G; Video S5). A particularly strong background autofluorescence in the *bicat2* and *bicat1 bicat2* protoplasts was subtracted from the NTRC-R-GECO1 measurements (Figures 6J and S12H). Since CPA targets ECA,[62] we also investigated mutants for this Ca^{2+} transporter. *Arabidopsis* possesses four ECA paralogs (*ECA1–4*); however, we successfully obtained homozygous transfer DNA (T-DNA) insertion mutants only for *ECA1–ECA3*. ECA1 and ECA2 were reported to reside in endomembranes, likely the ER membrane,[64,65] while ECA3 is targeted to the Golgi and post-Golgi compartments,[66,67] and proteomics evidence and prediction suggest that ECA4 localizes to the ER as well. Consistent with the CPA results (Figure 6F), but less pronounced, the *eca1*, *eca2*, and *eca3* mutants all exhibited a larger persistent $[Ca^{2+}]_{str}$ increase (Figures S12I–S12K). Although we cannot rule out a contribution from other Ca^{2+} stores such as the vacuole, considering the distinct $[Ca^{2+}]$ dynamics in stroma, cytosol, and ER, together with the strong effect of CPA, a known $[Ca^{2+}]_{ER}$ inhibitor and ECA target, and the altered response in chloroplast envelope- and ER/Golgi-residing Ca^{2+} transporters, it is likely that Ca^{2+} is transferred between the ER and chloroplast stroma, and this transfer is affected by HL exposure.

DISCUSSION

The fast $[Ca^{2+}]_{str}$ spike precedes all other Ca^{2+} signals and ROS accumulation

HL induced a fast $[Ca^{2+}]_{str}$ spike lasting no longer than 30 s, likely independent of ROS, as it occurred before H_2O_2 and $^1O_2$ accumulation (Figures 4A, 4B, and 4G). Moreover, the response was independent of light quality (Figures 3A and 3E) and only partially influenced by light intensity (Figures 3B and 3F). This suggests a distinct mechanism is responsible compared with the subsequent persistent $[Ca^{2+}]_{str}$ increase, which required greater light intensities and was largely intensity dependent. The fast $[Ca^{2+}]_{str}$ spike might be the result of an imbalance between light-induced stromal Ca^{2+} influx[68–70] and a hypothetical Ca^{2+} efflux to the ER, possibly due to reduced ER-resident Ca^{2+} ATPase activity. The drastic enhancement by CPA treatment (Figure 6F) and a concomitant dip of $[Ca^{2+}]_{ER}$ with the fast $[Ca^{2+}]_{str}$ spike (Figures 6D and S9G) support this hypothesis. Further research is needed to clarify why only certain chloroplasts experience a fast $[Ca^{2+}]_{str}$ spike and explore the physiological implications of this signal.

The persistent $[Ca^{2+}]_{str}$ increase is caused by HL stress, accompanied by photoinhibition and $^1O_2$ accumulation

Part of a biphasic Ca^{2+} response, the subsequent persistent $[Ca^{2+}]_{str}$ increase occurred together with hallmarks of HL stress, as the decrease of chlorophyll autofluorescence and Fv/Fm (Figures 4C and S7) indicated strong damage to the photosystems.[13] The persistent $[Ca^{2+}]_{str}$ increase was light dose dependent, occurring when light intensity exceeded 1,100 μmol photons m^{-2} s^{-1} (Figure S5), and was robustly triggered at 2,000 μmol photons m^{-2} s^{-1} (Figure 3; Table S1), typical of outdoor sunlight. Beyond 2,000 μmol photons m^{-2} s^{-1}, natural lensing conditions, such as water droplets, should be considered. While the effect of focused natural light on plant physiology is rarely studied,[4] focused sunlight spots are common in nature, e.g., on days with intermittent rain and sunshine (Figures 1A and 1B). We simulated this by focusing microscope light through a glass bead to trigger a persistent $[Ca^{2+}]_{str}$ increase (Figure 1C). Light focused through water droplets could create a "multiple dot effect," mimicking localized hypersensitive response-like cell death. In contrast, exposing a large area to white light likely triggers a more uniform, systemic stress response involving broader signaling and defense mechanisms. This suggests that localized and widespread light stress may engage distinct regulatory pathways. Specialized acclimation signaling, such as a stromal Ca^{2+} response, may be crucial to prevent sunburn and cell death,[71,72] warranting further study.

Our findings contradict previous research suggesting HL-induced H_2O_2 accumulation plays a role in the $[Ca^{2+}]_{str}$ response[40,73] as stromal H_2O_2 dynamics do not correlate in terms of kinetics or light intensity (Figures 4A and 4B). One counterargument is that an H_2O_2 threshold is required to induce the persistent $[Ca^{2+}]_{str}$ increase and that the sensor relies on endogenous E_{GSH} for re-generation, which is itself variable due to its various functions. Also, exogenous H_2O_2 application leads to a prolonged $[Ca^{2+}]_{str}$ elevation.[22,40] While H_2O_2 cannot be ruled out, pharmacological manipulation of the photosynthetic electron points to other ROS, such as $^1O_2$. Previously shown to

reduce H_2O_2 accumulation,[15,74] DCMU and DBMIB treatment actually accelerated the persistent $[Ca^{2+}]_{str}$ increase (Figures 4D and 4E). Additionally, while MV treatment previously enhanced stromal H_2O_2 accumulation,[47] the HL-induced $[Ca^{2+}]_{str}$ response was unaffected (Figure 4F). HL combined with DCMU boosts $^1O_2$ production at PSII, potentially leading to lipid peroxidation.[74] Our data show that $^1O_2$ accumulation closely aligns with the persistent $[Ca^{2+}]_{str}$ increase (Figures 4D and 4G). However, we cannot rule out the involvement of other HL-induced intermediates, beyond ROS, that may link photoinhibition and Ca^{2+} signaling.

HL-induced $[Ca^{2+}]_{str}$ kinetics differ between the epidermis, stomata, and mesophyll

A faster persistent $[Ca^{2+}]_{str}$ increase in epidermal chloroplasts (Figures 2B and 2E) may be linked to a recently identified class of specialized sensory plastids that are smaller, have more stromules, less complex grana stacking, and fewer plastoglobules than mesophyll chloroplasts.[75] They also differ in their proteome, featuring stress-related proteins. Interestingly, Beltran et al. noted changes in Ca^{2+}-signaling genes in cells containing sensory plastids, including calmodulin and rapid alkalinization factor-like elements.[76] These differences in chloroplast morphology may explain the distinct HL-induced $[Ca^{2+}]_{str}$ kinetics observed in different tissues.

However, we cannot rule out that light penetration differs between tissues/cell types and that the position of chloroplasts relative to the leaf surface determines the $[Ca^{2+}]_{str}$ response. Air pockets in the mesophyll scatter light, creating a light gradient within green tissues. An *abcg5* mutant was identified that increases hypocotyl transparency due to water-filled air pockets, causing light tropism defects that can be mimicked by water infiltration.[77] Interestingly, water infiltration impaired the persistent $[Ca^{2+}]_{str}$ increase, suggesting light scatter influences the HL response (Figure S10E). This effect may be further influenced by the leaf's internal light environment and the chloroplast avoidance response.[8] Light penetration differences may explain the variation between epidermal and mesophyll chloroplasts, but not the delayed response in stomata guard cell chloroplasts based on leaf depth.

The HL-induced $[Ca^{2+}]_{cyt}$ spike is an effect of a blue component in the white light spectrum

Blue and white light induced a cytosolic Ca^{2+} response, while red light had a minimal effect, indicating that blue light is likely more physiologically relevant for the HL response. The $[Ca^{2+}]_{cyt}$ peak was largely independent of light intensity (Figure 6C), suggesting that a blue light receptor such as phototropin[78–80] detects the blue spectrum in white light to induce the response. Interestingly, while Baum et al. reported a phototropin-dependent $[Ca^{2+}]_{cyt}$ peak, they did not observe a blue light-induced $[Ca^{2+}]_{str}$ increase, potentially due to differences in experimental setup.[80]

HL-induced systemic $[Ca^{2+}]$ elevations were reported previously but lacked subcellular information due to the use of the Ca^{2+} reporter dye FLUO4-AM.[81] The GCaMP3 reporter in the NTRC-R-GECO1 crossed line, along with a cyto-nuclear localized R-GECO1 line,[44] enabled us to observe an HL-induced nuclear $[Ca^{2+}]$ spike (Figure S9D; Video S4), potentially linking HL stress directly to gene expression and translation.[7,82,83] Recently, Moore et al. identified a translation-dependent retrograde signaling network regulated by MAP KINASE 6 (MPK6), SNF1 KINASE HOMOLOG 10 (AKIN10), STRESS ASSOCIATED PROTEINS (SAP) 2 and 3, and CALMODULIN-LIKE PROTEIN 49 (CML49) within minutes of HL exposure.[83] MPK6 can be activated by Ca^{2+} signals,[1] and CML49 contains Ca^{2+}-binding EF-hands, making them potential targets of the HL-induced nucleo-cytosolic $[Ca^{2+}]$ spike.

The HL-induced persistent $[Ca^{2+}]_{str}$ increase is conserved throughout the green lineage

Similar HL-induced $[Ca^{2+}]_{str}$ responses were observed in *Chlamydomonas* and *Phaeodactylum*.[39,40] Photoinhibition appears to drive the stromal Ca^{2+} response in all three organisms, correlating with ROS production. However, the fast $[Ca^{2+}]_{str}$ spike and $[Ca^{2+}]_{cyt}$ changes were not observed in *Chlamydomonas* or *Phaeodactylum*, possibly due to differences in setup or methodology, or vascular plants like *Arabidopsis* may have evolved a more complex HL-induced Ca^{2+} signature.

The ecological relevance of a burning glass effect in *Chlamydomonas* and *Phaeodactylum* is uncertain, as they typically inhabit soil and aquatic environments, respectively, with lower, diffuse light. However, rock pools and shallow water bodies could expose them to intense light and temperature fluctuations, potentially mimicking the burning glass effect. Additionally, water, soil particles like quartz, or diatom silica shells could concentrate light, increasing the risk of HL in low-light environments. Interestingly, even single cells like Synechocystis can function as microlenses, detecting and responding to light direction.[84] While initially discovered through natural lensing effects (Figure 1), Ca^{2+} responses occurred at light intensities similar to a typical sunny day, suggesting lensing may not be essential to trigger the response. Nevertheless, the response is strikingly similar, and we propose that a potential HL acclimation mechanism mediated by $[Ca^{2+}]_{str}$ accumulation has conserved evolutionary roots.

A potential origin and mechanism of the HL-induced $[Ca^{2+}]_{str}$ response

Our study led us to uncover an intimate connection between the ER and chloroplast Ca^{2+} pools that is disturbed upon HL exposure. This is summarized in a hypothetical model (Figure 7) and based on (1) $[Ca^{2+}]_{ER}$ mirroring the stromal response to HL (Figures 6D, 6E, and S9E–S9G); (2) CPA, a known inhibitor of ER-resident Ca^{2+}-ATPases, severely disrupting the HL-induced $[Ca^{2+}]_{str}$ response (Figure 6F); (3) in stomatal guard cells, CPA challenges in the absence of an HL stimulus leading to an opposing $[Ca^{2+}]$ dynamic in the ER and stroma and a lack of response in the cytosol (Figure S11); and (4) infiltration of water into the cotyledon, which likely minimizes internal light scatter and HL exposure, reducing both the HL-induced stromal and ER $[Ca^{2+}]$ increase and decrease, respectively (Figures S10E and S10F). This further indicates that light exposure drives the accumulation of Ca^{2+} in the ER. (5) Loss of function of the chloroplast envelope-located Ca^{2+}/Mn^{2+} transporter BICAT2 and the ER/Golgi-resident Ca^{2+}-ATPases, ECAs, alters the HL-induced $[Ca^{2+}]_{str}$ response (Figures 6J and S12). BICAT2 is evolutionarily conserved and essential for light-to-dark-induced $[Ca^{2+}]_{str}$ increase.[26,85] However, *bicat2* mutants are severely stunted and

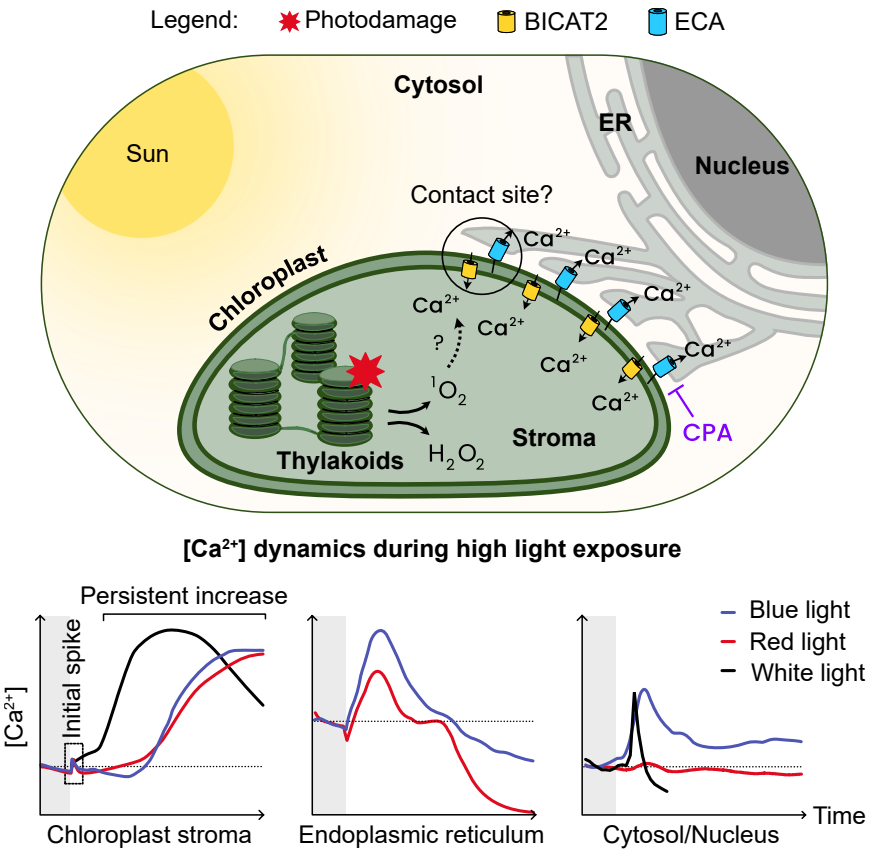

Figure 7. A hypothetical model of the HL-induced Ca^{2+} response in *Arabidopsis thaliana*

HL triggers a biphasic increase of $[Ca^{2+}]_{str}$ consisting of a fast initial Ca^{2+} spike that occurs in seemingly random chloroplasts, followed by a persistent Ca^{2+} increase in most chloroplasts. The $[Ca^{2+}]_{str}$ and $[Ca^{2+}]_{ER}$ responses are triggered irrespective of light wavelength, responding to both blue, red, and white light. The Ca^{2+} response in the cytosol and nucleus, however, is triggered only by blue and white light, which is likely a consequence of blue photoreceptor signaling. The fast $[Ca^{2+}]_{str}$ spike occurs before any detectable ROS signals. Therefore, we cannot conclude that ROS play a role in generating this signal. The persistent $[Ca^{2+}]_{str}$ increase, however, is a consequence of photodamage to the electron transport chain caused by HL and is likely the result of $^1O_2$, and not H_2O_2, altering a Ca^{2+} transfer between the ER and the chloroplast stroma that is potentially mediated by BICAT2 and ECA, and can be inhibited by CPA.

pale, making it unclear whether the impaired $[Ca^{2+}]_{str}$ response is due to disrupted Ca^{2+} transport or pleiotropic growth defects. In contrast, *eca* mutants displayed enhanced $[Ca^{2+}]_{str}$ responses, likely due to reduced Ca^{2+} export from the stroma to ER. The effect was milder than with CPA, possibly due to redundancy among the four ECA paralogs. The directionality of Ca^{2+} transfer is a key consideration. While for now, we lack strong evidence for a transfer of Ca^{2+} from the ER to the stroma, aside from the dip in $[Ca^{2+}]_{ER}$ during the fast $[Ca^{2+}]_{str}$ spike, the points discussed above suggest that HL inhibits the transfer of Ca^{2+} from the chloroplast stroma to the ER.

ER-chloroplast membrane contact sites (MCSs) are hubs for lipid exchange, supported by physical associations between the ER and chloroplasts.[58,86] More recently, ER-resident proteins VAP27-1 and VAP27-3 were identified as possible MCS tethers, with mutations leading to subtle changes in lipid composition.[87] While ER-mitochondria MCSs are known to regulate Ca^{2+} homeostasis in animal systems,[88] an equivalent mechanism in chloroplasts has not yet been established.

While the possibility of cytosolic Ca^{2+} contributing to the stromal signal cannot be entirely excluded, two points from our study preclude a direct transfer of the HL-induced $[Ca^{2+}]$ peak from cytosol to stroma that would result in the persistent $[Ca^{2+}]_{str}$ increase: a temporal mismatch between the $[Ca^{2+}]_{cyt}$ peak and persistent $[Ca^{2+}]_{str}$ increase (Figures 6D and S1C) and a lack of a red light-induced $[Ca^{2+}]_{cyt}$ peak under conditions that trigger the persistent $[Ca^{2+}]_{str}$ increase (Figure 6E). Furthermore, HL does not trigger a $[Ca^{2+}]_{cyt}$ peak in *Chlamydomonas* and *Phaeodactylum*.[39,40] We also cannot rule out a contribution of the thylakoid lumen to HL-induced $[Ca^{2+}]_{str}$ dynamics. Light-dependent Ca^{2+} uptake into the lumen, likely via BICAT1, is well supported, but evidence for Ca^{2+} release remains speculative.[26,89] Other proposed chloroplast Ca^{2+} stores, such as binding to stromal proteins or membrane phospholipids, seem unlikely. Similar to high-capacity Ca^{2+}-binding proteins like calreticulin in the ER, such mechanisms would be expected to yield elevated resting $[Ca^{2+}]_{str}$, which contrasts with the low nanomolar levels observed.[19] A direct role of the apoplast can be excluded, as EGTA treatment had little effect on the $[Ca^{2+}]_{str}$ response (Figure 6H). However, we cannot rule out a potential contribution from the vacuole.

The HL-induced $[Ca^{2+}]_{str}$ response appeared to be linked to photoinhibition and the production of ROS. ROS accumulates in the stroma; however, it is likely the accumulation in the cytosol or at the MCS membranes that perturbs the light-driven Ca^{2+} transfer between chloroplast and ER. Lipid peroxidation, driven by $^1O_2$ and detected in the chloroplast envelope and potentially other endomembranes, may modulate the activity of Ca^{2+} channels or transporters at the ER-chloroplast MCS. Such regulation is well-documented at ER-mitochondria MCS in animal systems[90,91] and may have parallels in plant cells.

Of note, while the HL-induced persistent $[Ca^{2+}]_{str}$ increase did not resemble a heat shock-induced $[Ca^{2+}]_{str}$ response, elevated temperatures did accelerate the HL response (Figure 5). The accelerated $[Ca^{2+}]_{str}$ response could be an effect of the generally enhanced rates of biochemical reactions at higher temperatures in the range of 10°C to 40°C.[92] A combined effect of heat on the HL-induced $[Ca^{2+}]_{str}$ response could be particularly relevant in the context of a warming climate in the future.[93]

In conclusion, inspired by the burning glass effect of water droplets on the leaf surface, our data support the existence

of ER-chloroplast Ca^{2+} exchange, mediated through specific transporters and influenced by photoinhibition and ROS. This mechanism may help plants acclimate to HL, offering potential new strategies to enhance photosynthesis and improve crop yields.

RESOURCE AVAILABILITY

Lead contact

Requests for further information and resources should be directed to and will be fulfilled by the lead contact, Simon Stael (simon.stael@slu.se).

Materials availability

Transgenic *Arabidopsis* lines and plasmids generated for this study will be made available upon request.

Data and code availability

- All data reported in this paper will be shared by the lead contact upon request.
- This paper does not report original code.
- Any additional information required to reanalyze the data reported in this paper is available from the lead contact upon request.

ACKNOWLEDGMENTS

This study was supported by the Knut and Alice Wallenberg Foundation (grant 2021.0071 to S.R. and S.S. and grant 2022.0029 to D.V. and M. Tenje), the European Research Council (Consolidator grant 101044878 to D.K., Q.Y., and S.S.), the Austrian Science Fund (Lise Meitner Program grant number M-2745-B to A.S.Z. and project P 37245-B to B.W. and M. Teige), the EU H2020-SFS-2019-2 RIA project ADAPT (GA 2020 862-858 to B.W. and M. Teige), the Ministero dell'Istruzione, dell'Università e della Ricerca Fondo per Progetti di Ricerca di Rilevante Interesse Nazionale 2022 (PRIN 2022NMSFHN) (to A.C. and S.B.), and by the Agritech National Research Center and received funding from the European Union Next-GenerationEU (PIANO NAZIO-NALE DI RIPRESA E RESILIENZA [PNRR]—MISSIONE 4 COMPONENTE 2, INVESTIMENTO 1.4-D.D. 1032 17/06/2022, CN00000022 to B.M.O.M.). Part of the work was carried out with the support of the NOLIMITS Center of Excellence for Plant Biology and Other Life Sciences established by the University of Milan. M.S. thanks the Deutsche Forschungsgemeinschaft (DFG) for funding (SCHW 1719/5-3, SCHW 1719/10-1, and SCHW 1719/11-1) and for the infrastructure grant INST 211/903-1 FUGG for the Zeiss LSM 980 confocal microscope as operated by the Imaging Network of the University of Münster (RI_00497). K.Z. thanks the China Scholarship Council (202006910019) for a personal PhD studentship. We thank Vincent Allouch for assistance with the design of the hypothetical model, various people for providing mutant *Arabidopsis* seeds as detailed in the material and methods, Melanie Krebs (Heidelberg University, Germany) for the pGPTVII-Bar-U-RGECO1 plasmid, and Jens Staal (VIB, Belgium) for the pICOz plasmid.

AUTHOR CONTRIBUTIONS

D.K., S.R., and S.S. designed the overall study, performed experiments, and wrote the manuscript with input from S.B., C.S., D.V.D., B.W., M.S., M. Teige, and A.C. M.S. and A.C. provided GECIs, other genetically encoded fluorescent reporters, and expertise on sensor usage protocols. A.S.Z., B.W., and M. Teige cloned and produced the NTRC- and AKDE1-R-GECO1-expressing *Arabidopsis* lines. B.M.O.M., S.B., and A.C. performed the soil-grown plant confocal imaging. K.Z. performed the automated white light system confocal microscopy experiments, supervised by M.S. E.M. and D.V.D. assisted D.K. with temperature shift experiments. Z.B. and M. Trtílek assisted S.R. with Fv/Fm measurements. Q.Y. cloned the transfection plasmid and assisted with protoplast assays. M.G. performed the CPA experiments in epidermal peels. D.V. and M. Tenje assisted with the thermocouple temperature measurements. All authors gave feedback on the manuscript.

DECLARATION OF INTERESTS

Z.B. is an employee of Photon Systems Instruments. M. Trtílek is a founder of Photon Systems Instruments and a member of its scientific advisory board.

DECLARATION OF GENERATIVE AI AND AI-ASSISTED TECHNOLOGIES IN THE WRITING PROCESS

During the preparation of this work, the authors used ChatGPT to condense the manuscript and refine sentence structure. After using this tool, the authors reviewed and edited the content as needed and take full responsibility for the content of the publication.

STAR★METHODS

Detailed methods are provided in the online version of this paper and include the following:

- KEY RESOURCES TABLE
- EXPERIMENTAL MODEL AND SUBJECT DETAILS
- METHOD DETAILS
  - Plasmid construction and transformation
  - Widefield microscopy
  - Confocal microscopy of *Arabidopsis* seedlings
  - Quantification of R-GECO1 and YC3.6 signals
  - 3D design and 3D printing
  - Confocal microscopy of soil-grown *Arabidopsis* plants
  - White light illumination and confocal microscopy
  - Confocal microscopy of protoplasts
  - Confocal and temperature-controlled microscopy
  - Analysis of calcium dynamics in guard cells
  - Protein extraction and immunoblotting
  - Measurement of photosynthetic parameters
- QUANTIFICATION AND STATISTICAL ANALYSIS

SUPPLEMENTAL INFORMATION

Supplemental information can be found online at https://doi.org/10.1016/j.cub.2025.04.065.

Received: September 28, 2024
Revised: March 16, 2025
Accepted: April 28, 2025
Published: May 20, 2025

REFERENCES

1. Matsumura, M., Nomoto, M., Itaya, T., Aratani, Y., Iwamoto, M., Matsuura, T., Hayashi, Y., Mori, T., Skelly, M.J., Yamamoto, Y.Y., et al. (2022). Mechanosensory trichome cells evoke a mechanical stimuli-induced immune response in Arabidopsis thaliana. Nat. Commun. *13*, 1216. https://doi.org/10.1038/s41467-022-28813-8.
2. Van Moerkercke, A., Duncan, O., Zander, M., Šimura, J., Broda, M., Vanden Bossche, R., Lewsey, M.G., Lama, S., Singh, K.B., Ljung, K., et al. (2019). A MYC2/MYC3/MYC4-dependent transcription factor network regulates water spray-responsive gene expression and jasmonate levels. Proc. Natl. Acad. Sci. USA *116*, 23345–23356. https://doi.org/10.1073/pnas.1911758116.
3. Bellenot, C., Routaboul, J.-M., Laufs, P., and Noël, L.D. (2022). Hydathodes. Curr. Biol. *32*, R763–R764. https://doi.org/10.1016/j.cub.2022.06.014.
4. Egri, A., Horváth, A., Kriska, G., and Horváth, G. (2010). Optics of sunlit water drops on leaves: conditions under which sunburn is possible. New Phytol. *185*, 979–987. https://doi.org/10.1111/j.1469-8137.2009.03150.x.

5. Dietz, K.J. (2015). Efficient high light acclimation involves rapid processes at multiple mechanistic levels. J. Exp. Bot. *66*, 2401–2414. https://doi.org/10.1093/jxb/eru505.

6. Ruban, A.V. (2016). Nonphotochemical Chlorophyll Fluorescence Quenching: Mechanism and Effectiveness in Protecting Plants from Photodamage. Plant Physiol. *170*, 1903–1916. https://doi.org/10.1104/pp.15.01935.

7. Suzuki, N., Devireddy, A.R., Inupakutika, M.A., Baxter, A., Miller, G., Song, L., Shulaev, E., Azad, R.K., Shulaev, V., and Mittler, R. (2015). Ultra-fast alterations in mRNA levels uncover multiple players in light stress acclimation in plants. Plant J. *84*, 760–772. https://doi.org/10.1111/tpj.13039.

8. Kasahara, M., Kagawa, T., Oikawa, K., Suetsugu, N., Miyao, M., and Wada, M. (2002). Chloroplast avoidance movement reduces photodamage in plants. Nature *420*, 829–832. https://doi.org/10.1038/nature01213.

9. Huang, J., Zhao, X., and Chory, J. (2019). The Arabidopsis Transcriptome Responds Specifically and Dynamically to High Light Stress. Cell Rep. *29*, 4186–4199.e3. https://doi.org/10.1016/j.celrep.2019.11.051.

10. Araguirang, G.E., and Richter, A.S. (2022). Activation of anthocyanin biosynthesis in high light - what is the initial signal? New Phytol. *236*, 2037–2043. https://doi.org/10.1111/nph.18488.

11. D'Alessandro, S., Beaugelin, I., and Havaux, M. (2020). Tanned or Sunburned: How Excessive Light Triggers Plant Cell Death. Mol. Plant *13*, 1545–1555. https://doi.org/10.1016/j.molp.2020.09.023.

12. Lee, H.N., Chacko, J.V., Gonzalez Solís, A., Chen, K.E., Barros, J.A.S., Signorelli, S., Millar, A.H., Vierstra, R.D., Eliceiri, K.W., and Otegui, M.S. (2023). The autophagy receptor NBR1 directs the clearance of photodamaged chloroplasts. eLife *12*, e86030. https://doi.org/10.7554/eLife.86030.

13. Aro, E.M., Virgin, I., and Andersson, B. (1993). Photoinhibition of Photosystem II. Inactivation, protein damage and turnover. Biochim. Biophys. Acta *1143*, 113–134. https://doi.org/10.1016/0005-2728(93)90134-2.

14. Mullineaux, P.M., Exposito-Rodriguez, M., Laissue, P.P., and Smirnoff, N. (2018). ROS-dependent signalling pathways in plants and algae exposed to high light: Comparisons with other eukaryotes. Free Radic. Biol. Med. *122*, 52–64. https://doi.org/10.1016/j.freeradbiomed.2018.01.033.

15. Exposito-Rodriguez, M., Laissue, P.P., Yvon-Durocher, G., Smirnoff, N., and Mullineaux, P.M. (2017). Photosynthesis-dependent H2O2 transfer from chloroplasts to nuclei provides a high-light signalling mechanism. Nat. Commun. *8*, 49. https://doi.org/10.1038/s41467-017-00074-w.

16. Mhamdi, A., and Van Breusegem, F. (2018). Reactive oxygen species in plant development. Development *145*, dev164376. https://doi.org/10.1242/dev.164376.

17. Shumbe, L., Chevalier, A., Legeret, B., Taconnat, L., Monnet, F., and Havaux, M. (2016). Singlet Oxygen-Induced Cell Death in Arabidopsis under High-Light Stress Is Controlled by OXI1 Kinase. Plant Physiol. *170*, 1757–1771. https://doi.org/10.1104/pp.15.01546.

18. Beaugelin, I., Chevalier, A., D'Alessandro, S., Ksas, B., Novák, O., Strnad, M., Forzani, C., Hirt, H., Havaux, M., and Monnet, F. (2019). OXI1 and DAD Regulate Light-Induced Cell Death Antagonistically through Jasmonate and Salicylate Levels. Plant Physiol. *180*, 1691–1708. https://doi.org/10.1104/pp.19.00353.

19. Stael, S., Wurzinger, B., Mair, A., Mehlmer, N., Vothknecht, U.C., and Teige, M. (2012). Plant organellar calcium signalling: an emerging field. J. Exp. Bot. *63*, 1525–1542. https://doi.org/10.1093/jxb/err394.

20. Hochmal, A.K., Schulze, S., Trompelt, K., and Hippler, M. (2015). Calcium-dependent regulation of photosynthesis. Biochim. Biophys. Acta *1847*, 993–1003. https://doi.org/10.1016/j.bbabio.2015.02.010.

21. Nomura, H., Komori, T., Uemura, S., Kanda, Y., Shimotani, K., Nakai, K., Furuichi, T., Takebayashi, K., Sugimoto, T., Sano, S., et al. (2012). Chloroplast-mediated activation of plant immune signalling in Arabidopsis. Nat. Commun. *3*, 926. https://doi.org/10.1038/ncomms1926.

22. Sello, S., Moscatiello, R., Mehlmer, N., Leonardelli, M., Carraretto, L., Cortese, E., Zanella, F.G., Baldan, B., Szabò, I., Vothknecht, U.C., et al. (2018). Chloroplast Ca(2+) Fluxes into and across Thylakoids Revealed by Thylakoid-Targeted Aequorin Probes. Plant Physiol. *177*, 38–51. https://doi.org/10.1104/pp.18.00027.

23. Sello, S., Perotto, J., Carraretto, L., Szabò, I., Vothknecht, U.C., and Navazio, L. (2016). Dissecting stimulus-specific Ca2+ signals in amyloplasts and chloroplasts of Arabidopsis thaliana cell suspension cultures. J. Exp. Bot. *67*, 3965–3974. https://doi.org/10.1093/jxb/erw038.

24. Teardo, E., Carraretto, L., Moscatiello, R., Cortese, E., Vicario, M., Festa, M., Maso, L., De Bortoli, S., Calì, T., Vothknecht, U.C., et al. (2019). A chloroplast-localized mitochondrial calcium uniporter transduces osmotic stress in Arabidopsis. Nat. Plants *5*, 581–588. https://doi.org/10.1038/s41477-019-0434-8.

25. Sai, J., and Johnson, C.H. (2002). Dark-stimulated calcium ion fluxes in the chloroplast stroma and cytosol. Plant Cell *14*, 1279–1291. https://doi.org/10.1105/tpc.000653.

26. Frank, J., Happeck, R., Meier, B., Hoang, M.T.T., Stribny, J., Hause, G., Ding, H., Morsomme, P., Baginsky, S., and Peiter, E. (2019). Chloroplast-localized BICAT proteins shape stromal calcium signals and are required for efficient photosynthesis. New Phytol. *221*, 866–880. https://doi.org/10.1111/nph.15407.

27. Martí Ruiz, M.C., Jung, H.J., and Webb, A.A.R. (2020). Circadian gating of dark-induced increases in chloroplast- and cytosolic-free calcium in Arabidopsis. New Phytol. *225*, 1993–2005. https://doi.org/10.1111/nph.16280.

28. Wang, C., Xu, W., Jin, H., Zhang, T., Lai, J., Zhou, X., Zhang, S., Liu, S., Duan, X., Wang, H., et al. (2016). A Putative Chloroplast-Localized Ca 2+ /H + Antiporter CCHA1 Is Involved in Calcium and pH Homeostasis and Required for PSII Function in Arabidopsis. Mol. Plant *9*, 1183–1196. https://doi.org/10.1016/j.molp.2016.05.015.

29. Schneider, A., Steinberger, I., Herdean, A., Gandini, C., Eisenhut, M., Kurz, S., Morper, A., Hoecker, N., Rühle, T., Labs, M., et al. (2016). The Evolutionarily Conserved Protein PHOTOSYNTHESIS AFFECTED MUTANT71 Is Required for Efficient Manganese Uptake at the Thylakoid Membrane in Arabidopsis. Plant Cell *28*, 892–910. https://doi.org/10.1105/tpc.15.00812.

30. Eisenhut, M., Hoecker, N., Schmidt, S.B., Basgaran, R.M., Flachbart, S., Jahns, P., Eser, T., Geimer, S., Husted, S., Weber, A.P.M., et al. (2018). The Plastid Envelope CHLOROPLAST MANGANESE TRANSPORTER1 Is Essential for Manganese Homeostasis in Arabidopsis. Mol. Plant *11*, 955–969. https://doi.org/10.1016/j.molp.2018.04.008.

31. Völkner, C., Holzner, L.J., Day, P.M., Ashok, A.D., Vries, J., Bölter, B., and Kunz, H.H. (2021). Two plastid POLLUX ion channel-like proteins are required for stress-triggered stromal Ca2+release. Plant Physiol. *187*, 2110–2125. https://doi.org/10.1093/plphys/kiab424.

32. Navazio, L., Formentin, E., Cendron, L., and Szabò, I. (2020). Chloroplast Calcium Signaling in the Spotlight. Front. Plant Sci. *11*, 186. https://doi.org/10.3389/fpls.2020.00186.

33. Vainonen, J.P., Sakuragi, Y., Stael, S., Tikkanen, M., Allahverdiyeva, Y., Paakkarinen, V., Aro, E., Suorsa, M., Scheller, H.V., Vener, A.V., et al. (2008). Light regulation of CaS, a novel phosphoprotein in the thylakoid membrane of *Arabidopsis thaliana*. FEBS Journal *275*, 1767–1777. https://doi.org/10.1111/j.1742-4658.2008.06335.x.

34. Stael, S., Rocha, A.G., Wimberger, T., Anrather, D., Vothknecht, U.C., and Teige, M. (2012). Cross-talk between calcium signalling and protein phosphorylation at the thylakoid. J. Exp. Bot. *63*, 1725–1733. https://doi.org/10.1093/jxb/err403.

35. Cutolo, E., Parvin, N., Ruge, H., Pirayesh, N., Roustan, V., Weckwerth, W., Teige, M., Grieco, M., Larosa, V., and Vothknecht, U.C. (2019). The High Light Response in Arabidopsis Requires the Calcium Sensor Protein CAS, a Target of STN7- and STN8-Mediated Phosphorylation. Front. Plant Sci. *10*, 974. https://doi.org/10.3389/fpls.2019.00974.

36. Petroutsos, D., Busch, A., Janssen, I., Trompelt, K., Bergner, S.V., Weinl, S., Holtkamp, M., Karst, U., Kudla, J., and Hippler, M. (2011). The chloroplast calcium sensor CAS is required for photoacclimation in Chlamydomonas reinhardtii. Plant Cell *23*, 2950–2963. https://doi.org/10.1105/tpc.111.087973.

37. Hochmal, A.K., Zinzius, K., Charoenwattanasatien, R., Gäbelein, P., Mutoh, R., Tanaka, H., Schulze, S., Liu, G., Scholz, M., Nordhues, A., et al. (2016). Calredoxin represents a novel type of calcium-dependent sensor-responder connected to redox regulation in the chloroplast. Nat. Commun. *7*, 11847. https://doi.org/10.1038/ncomms11847.

38. Zinzius, K., Marchetti, G.M., Fischer, R., Milrad, Y., Oltmanns, A., Kelterborn, S., Yacoby, I., Hegemann, P., Scholz, M., and Hippler, M. (2023). Calredoxin regulates the chloroplast NADPH-dependent thioredoxin reductase in Chlamydomonas reinhardtii. Plant Physiol. *193*, 2122–2140. https://doi.org/10.1093/plphys/kiad426.

39. Flori, S., Dickenson, J., Gaikwad, T., Cole, I., Smirnoff, N., Helliwell, K.E., Brownlee, C., and Wheeler, G.L. (2024). Diatoms exhibit dynamic chloroplast calcium signals in response to high light and oxidative stress. Plant Physiol. *197*, kiae591. https://doi.org/10.1093/plphys/kiae591.

40. Pivato, M., Grenzi, M., Costa, A., and Ballottari, M. (2023). Compartment-specific Ca(2+) imaging in the green alga Chlamydomonas reinhardtii reveals high light-induced chloroplast Ca(2+) signatures. New Phytol. *240*, 258–271. https://doi.org/10.1111/nph.19142.

41. Loro, G., Wagner, S., Doccula, F.G., Behera, S., Weinl, S., Kudla, J., Schwarzländer, M., Costa, A., and Zottini, M. (2016). Chloroplast-Specific in Vivo Ca2+ Imaging Using Yellow Cameleon Fluorescent Protein Sensors Reveals Organelle-Autonomous Ca2+ Signatures in the Stroma. Plant Physiol. *171*, 2317–2330. https://doi.org/10.1104/pp.16.00652.

42. Barton, K.A., Schattat, M.H., Jakob, T., Hause, G., Wilhelm, C., Mckenna, J.F., Máthé, C., Runions, J., Van Damme, D., and Mathur, J. (2016). Epidermal Pavement Cells of Arabidopsis Have Chloroplasts. Plant Physiol. *171*, 723–726. https://doi.org/10.1104/pp.16.00608.

43. Zhao, Y., Araki, S., Wu, J., Teramoto, T., Chang, Y.F., Nakano, M., Abdelfattah, A.S., Fujiwara, M., Ishihara, T., Nagai, T., et al. (2011). An expanded palette of genetically encoded Ca^{2+} indicators. Science *333*, 1888–1891. https://doi.org/10.1126/science.1208592.

44. Keinath, N.F., Waadt, R., Brugman, R., Schroeder, J.I., Grossmann, G., Schumacher, K., and Krebs, M. (2015). Live Cell Imaging with R-GECO1 Sheds Light on flg22- and Chitin-Induced Transient [Ca(2+)] cyt Patterns in Arabidopsis. Mol. Plant *8*, 1188–1200. https://doi.org/10.1016/j.molp.2015.05.006.

45. Schwarzländer, M., Wagner, S., Ermakova, Y.G., Belousov, V.V., Radi, R., Beckman, J.S., Buettner, G.R., Demaurex, N., Duchen, M.R., Forman, H.J., et al. (2014). The 'mitoflash' probe cpYFP does not respond to superoxide. Nature *514*, E12–E14. https://doi.org/10.1038/nature13858.

46. Elsässer, M., Feitosa-Araujo, E., Lichtenauer, S., Wagner, S., Fuchs, P., Giese, J., Kotnik, F., Hippler, M., Meyer, A.J., and Maurino, V.G. (2020). Photosynthetic activity triggers pH and NAD redox signatures across different plant cell compartments. Preprint at bioRxiv. https://doi.org/10.1101/2020.10.31.363051.

47. Ugalde, J.M., Fuchs, P., Nietzel, T., Cutolo, E.A., Homagk, M., Vothknecht, U.C., Holuigue, L., Schwarzländer, M., Müller-Schüssele, S.J., and Meyer, A.J. (2021). Chloroplast-derived photo-oxidative stress causes changes in H_2O_2 and *E*GSH in other subcellular compartments. Plant Physiol. *186*, 125–141. https://doi.org/10.1093/plphys/kiaa095.

48. Nietzel, T., Elsässer, M., Ruberti, C., Steinbeck, J., Ugalde, J.M., Fuchs, P., Wagner, S., Ostermann, L., Moseler, A., Lemke, P., et al. (2019). The fluorescent protein sensor roGFP2-Orp1 monitors in vivo H. New Phytol. New Phytol. *221*, 1649–1664. https://doi.org/10.1111/nph.15550.

49. Gutscher, M., Sobotta, M.C., Wabnitz, G.H., Ballikaya, S., Meyer, A.J., Samstag, Y., and Dick, T.P. (2009). Proximity-based Protein Thiol Oxidation by H2O2-scavenging Peroxidases. J. Biol. Chem. *284*, 31532–31540. https://doi.org/10.1074/jbc.M109.059246.

50. Fitzpatrick, D., Aro, E.-M., and Tiwari A, A. (2020). A Commonly Used Photosynthetic Inhibitor Fails to Block Electron Flow to Photosystem I in Intact Systems. Front. Plant Sci. *11*, 382. https://doi.org/10.3389/fpls.2020.00382.

51. Krieger-Liszkay, A., Fufezan, C., and Trebst, A. (2008). Singlet oxygen production in photosystem II and related protection mechanism. Photosynth. Res. *98*, 551–564. https://doi.org/10.1007/s11120-008-9349-3.

52. Lenzoni, G., and Knight, M.R. (2019). Increases in Absolute Temperature Stimulate Free Calcium Concentration Elevations in the Chloroplast. Plant Cell Physiol. *60*, 538–548. https://doi.org/10.1093/pcp/pcy227.

53. Moreau, D., Lefort, C., Burke, R., Leveque, P., and O'Connor, R.P. (2015). Rhodamine B as an optical thermometer in cells focally exposed to infrared laser light or nanosecond pulsed electric fields. Biomed. Opt. Express *6*, 4105–4117. https://doi.org/10.1364/BOE.6.004105.

54. Cantoni, F., Werr, G., Barbe, L., Porras, A.M., and Tenje, M. (2021). A microfluidic chip carrier including temperature control and perfusion system for long-term cell imaging. HardwareX *10*, e00245. https://doi.org/10.1016/j.ohx.2021.e00245.

55. Resentini, F., Ruberti, C., Grenzi, M., Bonza, M.C., and Costa, A. (2021). The signatures of organellar calcium. Plant Physiol. *187*, 1985–2004. https://doi.org/10.1093/plphys/kiab189.

56. Toyota, M., Spencer, D., Sawai-Toyota, S., Jiaqi, W., Zhang, T., Koo, A. J., Howe, G.A., and Gilroy, S. (2018). Glutamate triggers long-distance, calcium-based plant defense signaling. Science *361*, 1112–1115. https://doi.org/10.1126/science.aat7744.

57. Schattat, M., Barton, K., Baudisch, B., Klösgen, R.B., and Mathur, J. (2011). Plastid stromule branching coincides with contiguous endoplasmic reticulum dynamics. Plant Physiol. *155*, 1667–1677. https://doi.org/10.1104/pp.110.170480.

58. Andersson, M.X., Goksör, M., and Sandelius, A.S. (2007). Optical manipulation reveals strong attracting forces at membrane contact sites between endoplasmic reticulum and chloroplasts. J. Biol. Chem. *282*, 1170–1174. https://doi.org/10.1074/jbc.M608124200.

59. Mathur, J., Kroeker, O.F., Lobbezoo, M., and Mathur, N. (2022). The ER Is a Common Mediator for the Behavior and Interactions of Other Organelles. Front. Plant Sci. *13*, 846970. https://doi.org/10.3389/fpls.2022.846970.

60. Resentini, F., Grenzi, M., Ancora, D., Cademartori, M., Luoni, L., Franco, M., Bassi, A., Bonza, M.C., and Costa, A. (2021). Simultaneous imaging of ER and cytosolic Ca2+ dynamics reveals long-distance ER Ca2+ waves in plants. Plant Physiol. *187*, 603–617. https://doi.org/10.1093/plphys/kiab251.

61. Liiv, M., Vaarmann, A., Safiulina, D., Choubey, V., Gupta, R., Kuum, M., Janickova, L., Hodurova, Z., Cagalinec, M., Zeb, A., et al. (2024). ER calcium depletion as a key driver for impaired ER-to-mitochondria calcium transfer and mitochondrial dysfunction in Wolfram syndrome. Nat. Commun. *15*, 6143. https://doi.org/10.1038/s41467-024-50502-x.

62. Costa, A., Resentini, F., Buratti, S., and Bonza, M.C. (2023). Plant Ca2+-ATPases: From biochemistry to signalling. Biochim. Biophys. Acta Mol. Cell Res. *1870*, 119508. https://doi.org/10.1016/j.bbamcr.2023.119508.

63. Huang, S., Shen, L., Roelfsema, M.R.G., Becker, D., and Hedrich, R. (2023). Light-gated channelrhodopsin sparks proton-induced calcium release in guard cells. Science *382*, 1314–1318. https://doi.org/10.1126/science.adj9696.

64. Harper, J.F., Hong, B., Hwang, I., Guo, H.Q., Stoddard, R., Huang, J.F., Palmgren, M.G., and Sze, H. (1998). A novel calmodulin-regulated Ca2+-ATPase (ACA2) from Arabidopsis with an N-terminal autoinhibitory domain. J. Biol. Chem. *273*, 1099–1106. https://doi.org/10.1074/jbc.273.2.1099.

65. Liang, F., Cunningham, K.W., Harper, J.F., and Sze, H. (1997). ECA1 complements yeast mutants defective in Ca2+ pumps and encodes an endoplasmic reticulum-type Ca2+-ATPase in Arabidopsis thaliana.

Proc. Natl. Acad. Sci. USA *94*, 8579–8584. https://doi.org/10.1073/pnas.94.16.8579.

66. Mills, R.F., Doherty, M.L., López-Marqués, R.L., Weimar, T., Dupree, P., Palmgren, M.G., Pittman, J.K., and Williams, L.E. (2008). ECA3, a Golgi-localized P2A-type ATPase, plays a crucial role in manganese nutrition in Arabidopsis. Plant Physiol. *146*, 116–128. https://doi.org/10.1104/pp.107.110817.

67. Li, X., Chanroj, S., Wu, Z., Romanowsky, S.M., Harper, J.F., and Sze, H. (2008). A distinct endosomal Ca2+/Mn2+ pump affects root growth through the secretory process. Plant Physiol. *147*, 1675–1689. https://doi.org/10.1104/pp.108.119909.

68. Muto, S., Izawa, S., and Miyachi, S. (1982). Light-induced Ca2+ uptake by intact chloroplasts. FEBS Lett. *139*, 250–254. https://doi.org/10.1016/0014-5793(82)80863-6.

69. Kreimer, G., Melkonian, M., and Latzko, E. (1985). An electrogenic uniport mediates light-dependent Ca2+ influx into intact spinach chloroplasts. FEBS Lett. *180*, 253–258. https://doi.org/10.1016/0014-5793(85)81081-4.

70. Kreimer, G., Melkonian, M., Holtum, J.A., and Latzko, E. (1985). Characterization of calcium fluxes across the envelope of intact spinach chloroplasts. Planta *166*, 515–523. https://doi.org/10.1007/BF00391276.

71. Karpiński, S., Szechyńska-Hebda, M., Wituszyńska, W., and Burdiak, P. (2013). Light acclimation, retrograde signalling, cell death and immune defences in plants. Plant Cell Environ. *36*, 736–744. https://doi.org/10.1111/pce.12018.

72. Martienssen, R. (1997). Cell death: Fatal induction in plants. Curr. Biol. *7*, R534–R537. https://doi.org/10.1016/S0960-9822(06)00274-0.

73. Serena, F., Jack, D., Trupti, G., Isobel, C., Nicholas, S., Katherine, H., Colin, B., and Glen, W. (2023). Diatoms exhibit dynamic chloroplast calcium signals in response to high light and oxidative stress. Preprint at bioRxiv. https://doi.org/10.1101/2023.08.15.553405.

74. Exposito-Rodriguez, M., Reeder, B., Brooke, G.N., Hough, M.A., Laissue, P.P., and Mullineaux, P.M. (2024). A novel glutathione peroxidase-based biosensor disentangles differential subcellular accumulation of H2O2 and lipid hydroperoxides. Preprint at bioRxiv. https://doi.org/10.1101/2024.01.18.576236.

75. Mackenzie, S.A., and Mullineaux, P.M. (2022). Plant environmental sensing relies on specialized plastids. J. Exp. Bot. *73*, 7155–7164. https://doi.org/10.1093/jxb/erac334.

76. Beltrán, J., Wamboldt, Y., Sanchez, R., LaBrant, E.W., Kundariya, H., Virdi, K.S., Elowsky, C., and Mackenzie, S.A. (2018). Specialized Plastids Trigger Tissue-Specific Signaling for Systemic Stress Response in Plants. Plant Physiol. *178*, 672–683. https://doi.org/10.1104/pp.18.00804.

77. Nawkar, G.M., Legris, M., Goyal, A., Schmid-Siegert, E., Fleury, J., Mucciolo, A., De Bellis, D., Trevisan, M., Schueler, A., and Fankhauser, C. (2023). Air channels create a directional light signal to regulate hypocotyl phototropism. Science *382*, 935–940. https://doi.org/10.1126/science.adh9384.

78. Harada, A., Sakai, T., and Okada, K. (2003). Phot1 and phot2 mediate blue light-induced transient increases in cytosolic Ca2+ differently in Arabidopsis leaves. Proc. Natl. Acad. Sci. USA *100*, 8583–8588. https://doi.org/10.1073/pnas.1336802100.

79. Folta, K.M., Lieg, E.J., Durham, T., and Spalding, E.P. (2003). Primary inhibition of hypocotyl growth and phototropism depend differently on phototropin-mediated increases in cytoplasmic calcium induced by blue light. Plant Physiol. *133*, 1464–1470. https://doi.org/10.1104/pp.103.024372.

80. Baum, G., Long, J.C., Jenkins, G.I., and Trewavas, A.J. (1999). Stimulation of the blue light phototropic receptor NPH1 causes a transient increase in cytosolic Ca2+. Proc. Natl. Acad. Sci. USA *96*, 13554–13559. https://doi.org/10.1073/pnas.96.23.13554.

81. Fichman, Y., and Mittler, R. (2021). Integration of electric, calcium, reactive oxygen species and hydraulic signals during rapid systemic signaling in plants. Plant J. *107*, 7–20. https://doi.org/10.1111/tpj.15360.

82. Vogel, M.O., Moore, M., König, K., Pecher, P., Alsharafa, K., Lee, J., and Dietz, K.J. (2014). Fast retrograde signaling in response to high light involves metabolite export, MITOGEN-ACTIVATED PROTEIN KINASE6, and AP2/ERF transcription factors in Arabidopsis. Plant Cell *26*, 1151–1165. https://doi.org/10.1105/tpc.113.121061.

83. Moore, M., Smith, A.B., Wegener, M., Wesemann, C., Schmidtpott, S., Farooq, M.A., Ganguly, D.R., Seidel, T., Pogson, B.J., and Dietz, K.-J. (2022). Retrograde Control of Cytosolic Translation Targets Synthesis of Plastid Proteins and Nuclear Responses for High-Light Acclimation. Preprint at bioRxiv. https://doi.org/10.1101/2021.02.18.431817.

84. Schuergers, N., Lenn, T., Kampmann, R., Meissner, M.V., Esteves, T., Temerinac-Ott, M., Korvink, J.G., Lowe, A.R., Mullineaux, C.W., and Wilde, A. (2016). Cyanobacteria use micro-optics to sense light direction. eLife *5*, e12620. https://doi.org/10.7554/eLife.12620.

85. Kunz, H.H., Armbruster, U., Mühlbauer, S., de Vries, J., and Davis, G.A. (2024). Chloroplast ion homeostasis - what do we know and where should we go? New Phytol. *243*, 543–559. https://doi.org/10.1111/nph.19661.

86. Block, M.A., and Jouhet, J. (2015). Lipid trafficking at endoplasmic reticulum–chloroplast membrane contact sites. Curr. Opin. Cell Biol. *35*, 21–29. https://doi.org/10.1016/j.ceb.2015.03.004.

87. Renna, L., Stefano, G., Puggioni, M.P., Kim, S.-J., Lavell, A., Froehlich, J. E., Burkart, G., Mancuso, S., Benning, C., and Brandizzi, F. (2024). ER-associated VAP27-1 and VAP27-3 proteins functionally link the lipid-binding ORP2A at the ER-chloroplast contact sites. Nat. Commun. *15*, 6008. https://doi.org/10.1038/s41467-024-50425-7.

88. Loncke, J., Kaasik, A., Bezprozvanny, I., Parys, J.B., Kerkhofs, M., and Bultynck, G. (2021). Balancing ER-Mitochondrial Ca. Trends Cell Biol. *31*, 598–612. https://doi.org/10.1016/j.tcb.2021.02.003.

89. Ettinger, W.F., Clear, A.M., Fanning, K.J., and Peck, M.L. (1999). Identification of a Ca2+/H+ antiport in the plant chloroplast thylakoid membrane. Plant Physiol. *119*, 1379–1386. https://doi.org/10.1104/pp.119.4.1379.

90. Yoboue, E.D., Sitia, R., and Simmen, T. (2018). Redox crosstalk at endoplasmic reticulum (ER) membrane contact sites (MCS) uses toxic waste to deliver messages. Cell Death Dis. *9*, 331. https://doi.org/10.1038/s41419-017-0033-4.

91. Sassano, M.L., Tyurina, Y.Y., Diometzidou, A., Vervoort, E., Tyurin, V., More, S., Rovere, R.L., Giordano, F., Bultynck, G., Bayir, H., et al. (2024). Endoplasmic Reticulum-Mitochondria Contacts Are Apical Hotspots of Lipid Peroxidation Driving Ferroptosis. https://doi.org/10.21203/rs.3.rs-4311835/v1.

92. Ritchie, M.E. (2018). Reaction and diffusion thermodynamics explain optimal temperatures of biochemical reactions. Sci. Rep. *8*, 11105. https://doi.org/10.1038/s41598-018-28833-9.

93. Zandalinas, S.I., Fritschi, F.B., and Mittler, R. (2021). Global Warming, Climate Change, and Environmental Pollution: Recipe for a Multifactorial Stress Combination Disaster. Trends Plant Sci. *26*, 588–599. https://doi.org/10.1016/j.tplants.2021.02.011.

94. Kinoshita, T., Doi, M., Suetsugu, N., Kagawa, T., Wada, M., and Shimazaki, K. (2001). Phot1 and phot2 mediate blue light regulation of stomatal opening. Nature *414*, 656–660. https://doi.org/10.1038/414656a.

95. Guo, T., Liu, M., Chen, L., Liu, Y., Li, L., Li, Y., Cao, X., Mao, Z., Wang, W., and Yang, H.Q. (2023). Photoexcited cryptochromes interact with ADA2b and SMC5 to promote the repair of DNA double-strand breaks in Arabidopsis. Nat. Plants *9*, 1280–1290. https://doi.org/10.1038/s41477-023-01461-6.

96. Scholl, R.L., May, S.T., and Ware, D.H. (2000). Seed and molecular resources for Arabidopsis. Plant Physiol. *124*, 1477–1480. https://doi.org/10.1104/pp.124.4.1477.

97. Schindelin, J., Arganda-Carreras, I., Frise, E., Kaynig, V., Longair, M., Pietzsch, T., Preibisch, S., Rueden, C., Saalfeld, S., Schmid, B., et al. (2012). Fiji: an open-source platform for biological-image analysis. Nat. Methods *9*, 676–682. https://doi.org/10.1038/nmeth.2019.

98. Staal, J., Alci, K., De Schamphelaire, W., Vanhoucke, M., and Beyaert, R. (2019). Engineering a minimal cloning vector from a pUC18 plasmid backbone with an extended multiple cloning site. BioTechniques *66*, 254–259. https://doi.org/10.2144/btn-2019-0014.

99. Berg, S., Kutra, D., Kroeger, T., Straehle, C.N., Kausler, B.X., Haubold, C., Schiegg, M., Ales, J., Beier, T., Rudy, M., et al. (2019). ilastik: interactive machine learning for (bio)image analysis. Nat. Methods *16*, 1226–1232. https://doi.org/10.1038/s41592-019-0582-9.

100. Wu, F.-H., Shen, S.-C., Lee, L.-Y., Lee, S.-H., Chan, M.-T., and Lin, C.-S. (2009). Tape-Arabidopsis Sandwich - a simpler Arabidopsis protoplast isolation method. Plant Methods *5*, 16. https://doi.org/10.1186/1746-4811-5-16.

101. Prasad, A., Sedlářová, M., and Pospíšil, P. (2018). Singlet oxygen imaging using fluorescent probe Singlet Oxygen Sensor Green in photosynthetic organisms. Sci. Rep. *8*, 13685. https://doi.org/10.1038/s41598-018-31638-5.

STAR★METHODS

KEY RESOURCES TABLE

REAGENT or RESOURCE	SOURCE	IDENTIFIER
Antibodies		
RFP-tag primary antibody	GenScript	ref. A00682; RRID: AB_914506
horseradish peroxidase-conjugated anti-Rabbit secondary antibody	Agrisera	ref. AS09 602; RRID: AB_1966902
Bacterial and virus strains		
One Shot™ TOP10 Chemically Competent E. coli	Invitrogen	C404003
GV3101 Agrobacterium Chemically Competent Cells	GoldBio	CC-105-5x50
Chemicals, peptides, and recombinant proteins		
MitoView™ 405 dye (Biotium)	Biotum	70070
Dimethyl sulfoxide (DMSO)	Sigma-Aldrich	472301
3-(3,4-Dichlorophenyl)-1,1-dimethylurea, 97%, Thermo Scientific Chemicals (DCMU)	Thermo Fisher	L02986.18
Cyclopiazonic acid (CPA)	Sigma-Aldrich	C1530
2,5-Dibromo-6-isopropyl-3-methyl-1,4-benzoquinone (DBMIB)	Sigma-Aldrich	271993
Methyl viologen dichloride hydrate (MV)	Sigma-Aldrich	856177
Singlet Oxygen Sensor Green (SOSG)	Thermo Fisher	S36002
Methanol	Honeywell	34885
Ethylene glycol-bis(2-aminoethylether)-N,N,N,N-tetraacetic acid (EGTA)	Sigma-Aldrich	E3889
Polyethylene glycol 4000	Sigma-Aldrich	81240
Cellulase Onozuka R-10® from *Trichoderma viride ca.* 1 U/mg	SERVA	16419.02
Macerozyme R-10® from *Rhizopus sp.* lyophil.	SERVA	28302.02
Critical commercial assays		
ZymoPURE II Plasmid Midiprep Kit	ZYMO RESEARCH	D4200
Experimental models: Organisms/strains		
Arabidopsis thaliana: NTRC-R-GECO1	This study	N/A
Arabidopsis thaliana: AKDE-R-GECO1	This study	N/A
Arabidopsis thaliana: cyto-R-GECO1	Keinath et al.[44]	N/A
Arabidopsis thaliana: 2BAM4-YC3.6 (*rdr6* background)	Loro et al.[41]	N/A
Arabidopsis thaliana: NES-YC3.6 (*rdr6* background)	Loro et al.[41]	N/A
Arabidopsis thaliana: ER-GCaMP6-210	Resentini et al.[60]	N/A
Arabidopsis thaliana: cp-cpYFP	Schwarzländer et al.[45]	N/A
Arabidopsis thaliana: cyto-cpYFP	Schwarzländer et al.[45]	N/A
Arabidopsis thaliana: TKTP-Grx1-roGFP2	Ugalde et al.[47]	N/A
Arabidopsis thaliana: TKTP-roGFP2-Orp1	Ugalde et al.[47]	N/A
Arabidopsis thaliana: cyto-roGFP2-Orp1	Nietzel et al.[48]	N/A
Arabidopsis thaliana: cyto-nuclear GCaMP3	Toyota et al.[56]	N/A
Arabidopsis thaliana: NTRC-R-GECO1 x cyto-nuclear GCaMP3	This study	N/A
Arabidopsis thaliana: NTRC-R-GECO1 x ER-GCaMP6-210	This study	N/A
Arabidopsis thaliana: NTRC-R-GECO1 x TKTP-Grx1-roGFP2	This study	N/A
Arabidopsis thaliana: phot1-5 phot2-1	Kinoshita et al.[94]	N/A
Arabidopsis thaliana: cry1 cry2	Guo et al.[95]	N/A
Arabidopsis thaliana: bicat1-1	Frank et al.[26]	N/A
Arabidopsis thaliana: bicat2-1	Frank et al.[26]	N/A
Arabidopsis thaliana: bicat1-1 bicat2-1	Frank et al.[26]	N/A
Arabidopsis thaliana: Col-4 (WT)	Teardo et al.[24]	N/A

(*Continued on next page*)

Continued

REAGENT or RESOURCE	SOURCE	IDENTIFIER
Arabidopsis thaliana: cmcu-1 (Col-4 background)	Teardo et al.[24]	N/A
Arabidopsis thaliana: pec1-2 pec2-2	Volkner et al.[31]	N/A
Arabidopsis thaliana: eca1	Scholl et al.[96]	SALK_119898
Arabidopsis thaliana: eca2	Scholl et al.[96]	SALK_039146
Arabidopsis thaliana: eca3	Scholl et al.[96]	SALK_045567
Oligonucleotides		
*eca1*_LP: AAGTTTGAATAAAAACGGGGG	This study	N/A
*eca1*_RP: ACACGCATATCAGCAGGTACC	This study	N/A
*eca2*_LP: TGCTCTTCCAACTTCTTCACG	This study	N/A
*eca2*_RP: CAGAAGAACGCGATAGTGAGG	This study	N/A
*eca3*_LP: TCCGTGGAAAAAGATGTTGAC	This study	N/A
*eca3*_RP: GATGTCACCGAAACAATGGAG	This study	N/A
*eca4*_LP: TTCATCTGCTTCAAATACGCC	This study	N/A
*eca4*_RP: AGGCAGCTTTGAAGGTAAAGC	This study	N/A
*pec1-2*_LP: CGTACGCCAAAGATTTTGATC	This study	N/A
*pec1-2*_RP: GGAGCCAGACCTTTGATAAGG	This study	N/A
*pec2-2*_LP: CTTACCGATCACCTTTCGTTG	This study	N/A
*pec2-2*_RP: AAGCAAAAACAAATCTGGCAC	This study	N/A
*cmcu*_LP: TCCACAAGAGGGCATTTTTC	This study	N/A
*cmcu*_RP: TTTAGTGTTACCCCCGCATG	This study	N/A
Recombinant DNA		
Plasmid pGPTVII-Bar-NTRC-R-GECO1	This study	N/A
Plasmid pGPTVII-Bar-AKDE1-R-GECO1	This study	N/A
Plasmid pICOz-NTRC-R-GECO1	This study	N/A
Software and algorithms		
Prism	Graphpad	https://www.graphpad.com/features
Fiji	Schindelin et al.[97]	https://imagej.net/software/fiji/downloads
Fluorcam	Photon Systems Instruments	https://psi.cz/support/downloads/fc001/fkm001/

EXPERIMENTAL MODEL AND SUBJECT DETAILS

Arabidopsis chloroplast-localized GECI lines used in this study were NTRC-R-GECO1 (in Col-0 background) and 2BAM4-YC3.6 (in the *rdr6* background).[41] The cytosol-localized GECI lines were R-GECO1 (in Col-0 background, a kind gift from Dr. Melanie Krebs, Heidelberg University, Germany)[44] and NES-YC3.6 (in the *rdr6* background).[41] The ER-localized GECI was ER-GCaMP6-210.[60] As a pH sensor for the chloroplast stroma we employed cp-cpYFP, and for the cytosol cyto-cpYFP.[45] As chloroplast-localized sensors for glutathione redox potential (E_{GSH}) and H_2O_2 we selected TKTP-Grx1-roGFP2 and TKTP-roGFP2-Orp1, respectively,[47] and for sensing H_2O_2 in the cytosol cyto-roGFP2-Orp1.[48] The NTRC-R-GECO1 line was crossed with a cyto-nuclear localized GCaMP3 line[56] (a kind gift from Prof. Simon Gilroy, University of Wisconsin-Madison, USA, and Prof. Masatsugu Toyota, Saitama University, Japan), the ER-GCaMP6-210 line,[60] and the TKTP-Grx1-roGFP2 line.[47]

The following seeds were kindly gifted: The *phot1-5 phot2-1* mutant was originally reported in Kinoshita et al. (2001)[94] and gifted by Prof. John Christie (University of Glasgow, UK). The *cry1 cry2* mutant was from Prof. Hong-Quan Yang (Shanghai Normal University, China).[95] The *bicat1-1*, *bicat2-1*, and *bicat1-1 bicat2-1* mutants were from Prof. Edgar Peiter (Martin-Luther University Halle-Wittenberg, Germany).[26] The *cmcu-1* mutant and corresponding Col-4 wild type were from Prof. Ildikó Szabó (University of Padova, Italy).[24] The *pec1-2 pec2-2* mutant was from Prof. Hans-Henning Kunz (Ludwig Maximilian University of Munich, Germany).[31] Mutants *eca1* (SALK_119898), *eca2* (SALK_039146), and *eca3* (SALK_045567) were obtained from NASC.[96] For each line, the correct genotype was confirmed by PCR, or verified based on reported phenotype, prior to protoplast assays and imaging.

For cotyledons/roots imaging, *Arabidopsis* seedlings were grown on plates containing half-strength Murashige and Skoog medium (1/2 MS) with 0.8% plant agar under long-day conditions (16h light, 110 μmol photons m^{-2} s^{-1}, 22°C and 8 hours dark, 20°C) and a relative humidity of 60%. Imaging was conducted on 10- to 12-day-old seedlings.

To image soil-grown *Arabidopsis* plants using confocal laser scanning microscopy, NTRC-R-GECO1 seeds were sown directly in soil-filled 3.5 cm pots and kept at 4°C in the dark for 2 days to stratify. The pots were then transferred to the growth chamber under short-day conditions (12 hours light/12 hours dark, 100 μmol photons m^{-2} s^{-1}) at temperatures of 18-20°C and 75% relative humidity. Imaging experiments were conducted on 7- to 8-week-old plants, when the leaves were sufficiently large to fit the customized 3D-printed chamber.

For protoplast imaging, 10- to 12-day-old seedlings were transferred from plates to soil-filled 7 cm pots and grown to maturity for 5 to 7 weeks in a chamber under long day conditions of 150 μmol photons m^{-2} s^{-1} light for 16 h, 8 h dark, 22 °C, 70% humidity.

For imaging cotyledons in the light box setup, 2BAM4-YC3.6 expressing seedlings were grown on 1/2 MS medium supplemented with 0.8% agar under long-day conditions (16 h light, 30 μmol photons m^{-2} s^{-1}, 22°C and 8 hours dark, 18°C) after stratification at 4°C for two days. Plants were growing at a lower light intensity than other conditions to maximize the shift in light intensity to 600 or 1100 μmol photons m^{-2} s^{-1}.

METHOD DETAILS

Plasmid construction and transformation

NTRC-R-GECO1 and AKDE1-R-GECO1 plasmids were cloned with NEBuilder from synthetic fragments into a SpeI-ApaLI linearized vector, pGPTVII-Bar-U-RGECO1 (a kind gift from Dr. Melanie Krebs, Heidelberg University, Germany) (Figure S2B). Plasmids were introduced into *Arabidopsis* (Col-0) through the floral dip method and stable single T-DNA insertion homozygous lines were selected. NTRC-R-GECO1 and AKDE1-R-GECO1 lines were further selected that have a similar expression level as the original R-GECO1 line, assessed by western blot with an anti-RFP antibody (Figure S2E).

A HindIII-EcoRI fragment containing the ubiquitin-10 promoter and NTRC-R-GECO1 was subcloned to pICOz,[98] generating pICOz-NTRC-R-GECO1, which was used for protoplast transformations.

Widefield microscopy

Widefield microscopy was performed on a Nikon Eclipse Ti inverted microscope for Figures S1B and S1C. Samples were prepared under the low light of a desktop lamp. Cotyledons of 2BAM4-YC3.6 and NES-YC3.6 lines were detached and placed in imaging solution (5 mM KCl, 10 mM MES pH 5.8, and 10 mM $CaCl_2$) in a custom-made imaging chamber and overlaid with a slab of phytagel to image the abaxial side. Images were acquired with a 20x 0.75 NA dry objective and excitation of 436 +/- 20 nm, and emissions around 483 +/- 20 nm (CFP) and 542 +/- 20 nm (cpVenus). Images were analyzed using the ImageJ software package.[97] Ratios of cpVenus/CFP were calculated from average intensities of full frames minus a background subtraction, normalized to the pre-stimulus intensity, and plotted over time.

Confocal microscopy of *Arabidopsis* seedlings

Confocal laser scanning microscopy (CLSM) was performed on a Zeiss LSM 780 inverted confocal microscope unless stated otherwise. Images were acquired with a 20x 0.75 NA dry objective. Cotyledons and leaves from 10-12 days old *Arabidopsis* seedlings were detached, placed in distilled water on a microscope slide, and covered with a cover slip. For roots, the intact seedling was placed on a slide with distilled water, and covered with a cover slip with the shoot part hanging outside. To minimize later focus changes, samples were left to incubate under a desk lamp for at least 10 min before imaging. The pinhole was set at an aperture of 5 μm. The incubated samples were firstly imaged intermittently every 30 secs for 100 sec. As the exposure time for every image was 900 ms, the sample was illuminated for a relatively short period during the 30 sec interval. Hence, this period of 100 sec could be considered as a low light (not HL) treatment. Afterwards, samples were imaged every second for 600 sec. This period of 600 sec is considered as a continuous HL treatment, as the 900 ms exposure fills a relatively big part of the one second interval.

For blue and red light-induced Ca^{2+} imaging, both stroma- and cytosol-localized YC3.6 was excited with a 405 nm laser, and emission of the FRET pair CFP and cpVenus was collected at 465–500 nm and 525–560 nm, respectively. Different laser intensities of the 405 nm laser (5%, 7.5%, 10%, 20%) and of 633 nm laser (10%, 30%, 50%) were used as HL stimuli. Laser power (W) was measured using a power meter (Thorlabs Microscope Slide Power Meter, PM400 power meter console and S170C sensor head). The corresponding light intensities (μmol photons m^{-2} s^{-1}) were calculated (Table S1). Laser power was measured periodically to ensure similar light intensity, as laser strength decays over time. Both stroma/cytosol-localized R-GECO1 was excited with a 1% 561 nm laser, emission was collected at 580–630 nm. Along with the excitation light, a 10% 405 nm or a 30% 633 nm laser was used as HL stimulus. The imaging protocols of R-GECO1 and YC3.6 were also used on Col-0 plants, to exclude the potential influence of chlorophyll autofluorescence. For blue light-induced ER Ca^{2+} imaging, ER-localized ER-GCaMP6-210, was sequentially excited by a 10% 405 nm laser and a 20% 488 nm laser, emission was collected at 500–550 nm; for red light-induced ER Ca^{2+} imaging, ER-GCaMP6-210 was sequentially excited by a 3% 405 nm laser and a 3% 488 nm laser, with an additional constant 30% 633 nm laser as the HL stimulus. Cytosol-localized GCaMP3 of the NTRC-R-GECO1 × cyto-GCaMP3 line was excited with a 1% 488 nm laser, emission was collected at 500–550 nm. R-GECO1 was imaged as mentioned above with an additional 10% 405 nm laser as the HL stimulus. Chlorophyll autofluorescence was collected at an emission of 650–720 nm.

For blue light-induced ROS imaging, cotyledons of TKTP-roGFP2-Orp1 and cyt-roGFP2-Orp1 expressing plants were imaged with the same light regime as 2BAM4-YC3.6 for a correct comparison in Figure 4. Cotyledons were excited sequentially with a 405 nm diode laser and a 488 nm white light laser on a Leica SP8 CSLM, with a 40x water immersion objective. For roGFP2-Orp1, emission was collected at 500-527 nm in both sequences, which is required for ratiometric imaging of roGFP2 oxidation/reduction. For YC3.6, 455-483 nm (CFP) and 514-542 nm (cpVenus) emission was collected in the 405 nm excitation sequence, required for ratiometric Ca^{2+} imaging, and emission was set out of range for the 488 nm excitation, because this excitation was needed to have an equal input of laser strength as roGFP2-Orp1 and not for imaging. Two rounds of experiments were carried out, first with 9.94% of 405 nm and 11% of 488 nm excitation, and secondly with 20% 405 nm and 22% 488 nm excitation. Cotyledons of stroma-localized glutathione redox potential (E_{GSH}) sensor, TKTP-Grx1-roGFP2, were sequentially excited with a 405 nm and a 488 nm laser (energy equals to 10% 405 nm laser), emission was collected at 510-535 nm on the Zeiss LSM 780.

Stromal pH was measured as a control for the stroma-localized R-GECO1 reporter with a cp-cpYFP reporter on the Zeiss LSM 780. cpYFP was sequentially excited with a 405 nm and a 488 nm laser (energy equals to 10% 405 nm laser), emission was collected at 510-535 nm.

For quantification, average intensities of full frames were calculated with ImageJ,[97] data were normalized to the average baseline intensity, and plotted over time.

Quantification of R-GECO1 and YC3.6 signals

Regions of interest (ROIs) were drawn around groups of chloroplasts corresponding to a specific tissue (mesophyll, epidermis, and stomata) based on their morphological differences, or around single chloroplasts, using ImageJ. ROIs were drawn around single nuclei for cyt-R-GECO1 based on their typical shape (Figure S9A) and behavior (lack of movement or cytoplasmic streaming). Average signal intensity per ROI was measured over time for R-GECO1 and YC3.6 and was normalized by dividing all values per time series by the average of values of the baseline. To quantify the effect of different laser strengths, the parameters 'area under the curve' (AUC) and 'time to reach max' (TRM) were calculated.

3D design and 3D printing

To image soil-grown *Arabidopsis* plants with an upright CLSM, we designed a dedicated 3D-printed chamber. The chamber was designed using the Fusion 360 3D CAD software (Autodesk, https://www.autodesk.com/). The 3D models were exported in standard tessellation language (STL) format and post-processed with the open-source slicing engine Cura (Ultimaker, https://ultimaker.com/software/ultimaker-cura). Chambers were printed with a Kobra 3D printer (Anycubic, https://store.anycubic.com/products/kobra) at 0.2 mm resolution and 100% infill in PETG standard plastic filament.

The chamber was designed for single-cell imaging of soil-grown *Arabidopsis* leaves while keeping them attached to the plants in their pots. To achieve this, the chamber was designed to keep the imaged leaf as flat as possible, a crucial requirement for using the Water Dipping Objective (Nikon CFI75 Apo 25XC W 1300) to focus on single cells. This was accomplished by designing a pot casing with a support similar to a "trampoline" to hold the leaf. To prevent damage to the leaf lamina, the surfaces of the "trampoline" that contact the leaf were covered with cotton strips. When short-day-grown *Arabidopsis* plants in their pots were transferred to the imaging chamber, a large rosette leaf was secured to the holder with two braces and placed on the microscopy stage under the objective (Figure S3A).

Confocal microscopy of soil-grown *Arabidopsis* plants

CLSM analyses were performed using a Nikon A1R laser scanning confocal mounted on a Nikon ECLIPSE FN1 upright microscope with a Water Dipping Objective (Nikon CFI75 Apo 25XC W 1300). Images were acquired at 512 x 512 pixels with 5X digital zoom. NTRC-R-GECO1 was excited by a 561 nm single-mode optical fiber laser, and the emission was collected at 580-630 nm. The 561 nm laser line was set to 1%, corresponding to an incident power of 26 μW measured on the sample with the 25X objective (Table S1).

Different experiments were conducted. As a control, plants expressing NTRC-R-GECO1 were illuminated with the 561 nm laser set to 1% every 5 secs for 16 min. For HL stress experiments, two conditions were tested: i) plants expressing NTRC-R-GECO1 were illuminated with the 561 nm laser set to 1% every 5 secs for 3 min, followed by 3 min of continuous illumination, and then 10 min of illumination and acquisition every 5 secs; ii) plants expressing NTRC-R-GECO1 were illuminated with the 561 nm laser set to 1% every 5 secs for 3 min, followed by 3 min of continuous illumination with the 561 nm set to 1% laser coupled with 405 nm illumination (set to 20%, corresponding to 115-120 μW), and then 10 min of illumination with the sole 561 nm laser set to 1% and acquisition every 5 secs.

Images were analyzed using IMAGEJ software, and pixel intensities were measured over ROIs drawn on single chloroplasts. NTRC-R-GECO1 emissions were used for calculations, normalized to the pre-stimulus intensity, and plotted against time. Images in Figure S4 and Video S3 were denoised using the NIS-Element Denoise.ai plugin (https://www.microscope.healthcare.nikon.com/en_EU/products/confocal-microscopes/a1hd25-a1rhd25/nis-elements-ai). Only non-denoised images were analyzed for fluorescence quantification using Fiji.[97]

White light illumination and confocal microscopy

For manual white light-induced Ca^{2+} imaging, the epifluorescence light source of the Zeiss LSM780 CLSM, a mercury short-arc lamp (HXP 120 V), was used to expose the cotyledons of 2BAM4-YC3.6 expressing plants to white light (Figure 3I). For Figure 1, the

transmitted light, a Zeiss HAL 100 Halogen lamp, was used as a source of white light on the Zeiss LSM780 CLSM. To lens the transmitted light, a glass bead of 5 mm diameter was glued to the microscope slide on top of the position of the mounted cotyledon. Images were taken each minute by switching manually between white light (around 50 sec) and acquisition mode (around 10 sec). Images were taken and data processed as explained previously for plate-grown *Arabidopsis* seedlings.

For Figure S4, the transmitted light, a Zeiss HAL 100 Halogen lamp, was used as a source of white light on a Zeiss LSM710 inverted confocal microscope with a C-Apochromat 40x/1.20 W Korr M27 objective. Cotyledons of 2BAM4-YC3.6 and NES-YC3.6 plants were switched from low light (10% transmitted light) to HL (100% transmitted light). Images were taken each minute by switching manually between white light (around 50 sec) and acquisition mode (around 10 sec) for 2BAM4-YC3.6 and each half a minute for NES-YC3.6. YC3.6 was excited with a 5% 405 nm laser, and emission of FRET pair proteins CFP and cpVenus was collected at 465-500 nm and 525-560 nm, respectively. For data in Figure S5 we performed plastid segmentation and tracking with Fiji and ilastik. Raw image files were opened in Fiji[97] and the chlorophyll autofluorescence channel only was selected for each time series using the slice keeper tool. The chlorophyll autofluorescence image series were saved in hdf5 format, without compression and in xyt dimensions, using the hdf5 image plugin from Fiji. The chlorophyll autofluorescence image series was then loaded into ilastik v1.4.0[99] as input data and pixel classification was started at the first image of each time series. For training, two labels were created: one for the background, one for chloroplasts. Thresholding was chosen that only non-overlapping plastids remained in the selection. This eliminated about half of the mesophyll plastid signals since chloroplast crowding therein leads to merged objects but at the same time allows for more accurate tracking of the remaining single plastids. The tracking workflow was started by importing the series of images and the results of the pixel classification workflow. Following the ''animal tracking workflow'', chloroplasts were semi automatically tracked through the image series. First ~30 different chloroplasts were semi automatically tracked throughout a data set and then automatic tracking was used to follow the rest of the plastids throughout the datasets. The resulting object circumferences were used as masks to create ROIs on the CFP and cpVenus fluorescence channels in Fiji. Average fluorescence ratios for multiple single chloroplasts were plotted over time.

For On-stage white light stimuli, the 2BAM4-YC3.6 line was imaged during low light-to-high light transitions using a Zeiss LSM 980 microscope equipped with a 25X lens (Plan-Apochromat) (Carl Zeiss Microscopy GmbH, Jena, Germany). Cotyledons of 15-day old seedlings were cut and mounted between two coverslips (18 x 18 mm and 22 x 40 mm, VWR International GmbH, Darmstadt, Germany). The light box setup was previously described in detail in Elsässer et al.[46] Shortly, a customized on-stage illumination system was connected to the LSM 980 via the Zeiss trigger interface, enabling control of the microscope and the illumination system in a coordinated manner using the Experiment Designer in ZEN blue 3.5. A custom-built device (workshop, Institute for Geoinformatics, University of Münster, Germany) uses a 5 V trigger signal to switch a cold-white LED (Optonica GmbH, Salzburg, Germany) implemented in the on-stage illumination system. Images (1.26 sec per scan) were taken automatically with a 30 sec interval during which the sample is exposed to LED light. YC3.6 fluorescence was excited at 445 nm, while emission was collected at 473-490 nm (CFP) and 535-552 nm (cpVenus). The pinhole was set to 600 μm. The CLSM time series datasets were processed with a custom MATLAB-based software110 using x,y noise filtering. Ratios were then $\log_{10}$-transformed before statistical analysis was performed using GraphPad Prism (version 8.0.1, GraphPad Software, San Diego, CA, USA).

Confocal microscopy of protoplasts

Protoplasts were isolated from 5- to 6-week-old plants using the Tape-*Arabidopsis* Sandwich method.[100] Protoplasts isolated from the NTRC-R-GECO1 line were imaged on a Zeiss LSM 780 microscope with a 20X 0.75 NA dry objective. R-GECO1 was excited with a 1% 561 nm laser, emission was collected at 580-630 nm. A mercury short-arc lamp (HXP 120 V) was used for white high light stimuli. Protoplasts were firstly imaged every 30 sec without white light (baseline), afterwards, images were taken each minute by switching manually between white light (50 sec) and acquisition mode (10 sec). Chemical treatments on protoplast system: 10 μM 3-(3,4-dichlorophenyl)-1,1-dimethylurea (DCMU), 10 μM 2,5-Dibromo-6-isopropyl-3-methyl-1,4-benzoquinone (DBMIB), 50 μM methyl viologen (MV), 25 μM Cyclopiazonic acid (CPA), 10 mM ethylene glycol tetraacetic acid (EGTA). Protoplasts were kept in W5 solution (154 mM NaCl, 125 mM $CaCl_2$, 5 mM KCl, 5 mM glucose, and 2 mM MES, pH 5.7) for all measurements, except in combination with EGTA, where we used MMg solution (0.4 M mannitol, 15 mM MgCl2, and 4 mM MES, pH 5.7). For quantification, average intensities of full frames were calculated with Fiji,[97] data were normalized to the average baseline intensity, and plotted over time.

Protoplasts isolated from Col-0 plants were incubated with 100 μM Singlet Oxygen Sensor Green (SOSG) for 90 min. SOSG was excited with a 1% 488 nm laser, emission was collected at 500-600 nm on the Zeiss LSM 780 with a 20X 0.75 NA dry objective. The white light treatment was applied as mentioned above for NTRC-R-GECO1 protoplasts. Protoplasts without SOSG incubation were imaged using the same protocol to exclude the effect of chlorophyll autofluorescence. For quantification, average intensities of selected protoplasts were calculated with Fiji.[97] SOSG has a tendency for photosensitization in white light leading to an increased background signal.[101] Hence, background subtraction was performed for quantification. Nevertheless, the signal that overlapped with chloroplast localization was stronger than the background. After background subtraction, data were normalized to the average baseline values, and plotted over time.

Mitochondria of protoplasts were stained with the MitoView™ 405 dye (Biotium) at a concentration of 200 nM. The protoplasts were incubating for 15 min before imaging.

Protoplasts derived from mutant *Arabidopsis* plants were transformed with pICOz-NTRC-R-GECO1 plasmid. Due to its compact size (1185 bp), pICOz is an ideal backbone for minimizing the final plasmid size (3560 bp, including the ubiquitin-10 promoter and NTRC-R-GECO1), resulting in excellent protoplast transfection rates (~70%). Imaging was performed on a Leica Stellaris 5

microscope (for *cry1 cry2*, *pec1-2 pe2-2*, *cmcu*, *bicat1-1*, *bicat2-1*, *bicat1-1 bicat2-1*, *eca1*, *eca2*, *eca3*) and a Zeiss LSM 780 microscope (for *phot1-5 phot2-1*). The imaging settings for Zeiss LSM 780 microscope are mentioned above. For the Leica Stellaris 5 microscope, a 20X dry objective was used. R-GECO1 was excited with a 5% 561 nm laser and emission was collected at 580–630 nm. 100% of the 405 nm solid state laser was required as HL stimulus. Protoplasts were firstly imaged every 30 sec with sequential 5% 561 nm (400 msec) and 100% 405 nm (400 msec), afterwards, images were continuously taken every second for 12 minutes.

To ensure that light exposure did not result in heat shock, the temperature of the protoplast solution was monitored in a separate experiment using a thermocouple probe connected to a computer via an Arduino-based controller, as previously described.[54] The probe tip was mounted in water on a slide, similarly to how the protoplast slides were prepared, and temperature was calculated as a function of measured resistance through the thermocouple, under imaging conditions as mentioned above.

Confocal and temperature-controlled microscopy

Confocal spinning disk microscopy (CSDM) was performed on a Nikon Ti microscope with the Perfect Focus System (PFSIII) for Z-drift compensation, equipped with an Ultraview spinning-disk system (PerkinElmer) and two 512x512 Hamamatsu ImagEM C9100-13 EMccd cameras. Images were acquired using a 20X dry objective. Stromal Ca^{2+} imaging for 2BAM4-YC3.6 was carried out similar to the protocol mentioned above and the imaging setup is shown in Figure S8A. YC3.6 was excited at 10% 405 nm (149 μW), emission was passed through a 509 nm beam splitter and collected for CFP channel at 455-509 nm and cpVenus channel at 525-575 nm. Different temperature incubations (constant 10, 20, 30 or 40°C), temperature shifts (2-minute 20°C to 13-minute 40°C to 5-minute 20°C), and a constant 20°C during light shifts were performed with a CherryTemp heating/cooling system (Cherry Biotech). For the temperature incubation (Figure 5A), the light regime was switched from 2-minute intermittent imaging (once every 30 sec) to 13-minute continuous imaging; for temperature shifts / controls (Figures 5B, S8B, and S8C), the light regime was 20-minute intermittent imaging (once every 10 sec); for light shifts (Figure 5C), the light regime was switched from 2-minute intermittent imaging (once every 30 sec) to 13-minute continuous imaging to 5-minute intermittent imaging (once every 30 sec). The samples were incubated for 5 min on the CherryTemp system prior to imaging to stabilize the initial temperature.

Detached cotyledons were incubated in 100 μM rhodamine B solution or deionized water (control) for 30 minutes and briefly rinsed in deionized water prior to imaging. Temperature on the slide was changed with the CherryTemp system and was allowed to stabilize for 5 minutes prior to imaging. Rhodamine B was excited at 561 nm and emission collected at 580-650 nm. To mimic the 2BAM4-YC3.6 experiment in Figure 5C, cotyledons were sequentially exposed to 900 ms of 10% 405 nm (high light) and 25 ms of 561 nm (rhodamine B excitation light).

Analysis of calcium dynamics in guard cells

CSDM analyses of guard cells were performed using a Nikon Eclipse Ti2 inverted microscope, equipped with a Yokogawa Spinning Disk Confocal System. Images were acquired with a 60X 1.4 NA oil immersion objective. A central portion of a mature leaf of 4-week-old plants was attached to a cover slide using double-sided tape. A razor blade was used to gently remove upper cell layers. Isolated strips of the lower cell layer were incubated in the imaging solution (10 mM MES, 5 mM KCl, 50 μM $CaCl_2$, pH 6.15 adjusted with Tris-base) and left in dark for 15 minutes prior to acquisition. Stroma- and cytosol-localized R-GECO1 were excited with a 70% 561 laser for 100 ms and the emission was collected at 576–626 nm. ER-localized ER-GCaMP6-210 was excited with a 70% 488 laser for 200 ms and the emission was collected at 525–550 nm. Images were acquired every minute. 25 μM cyclopiazonic acid (CPA) and 0.25% dimethyl sulfoxide (DMSO) treatments were administered from a 2X working solution at 5 min from the start of the experiment. CPA and DMSO were prepared as follows: CPA was dissolved in 100% dimethyl sulfoxide at a concentration of 10 mM, and diluted at a concentration of 50 μM (2X) in the imaging solution; 100% dimethyl sulfoxide was diluted at a concentration of 0.50% (2X) in the imaging solution. Images were analyzed using Fiji software, and pixel intensities were measured over ROIs drawn on single guard cells. Emissions were normalized to the pre-stimulus intensity as $(F\text{-}F_0)/F_0$ and plotted over time. Images were denoised using the NIS-Element Denoise.ai plugin (Nikon) for visualization in Figures S11A–S11E. Only non-denoised images were analyzed for fluorescence quantification using Fiji.[97]

Protein extraction and immunoblotting

Protein extraction and immunoblotting were performed on 25 bulked seedlings. Total protein extraction was performed with Laemmli extraction buffer (0.0625 M Tris base; 0.07 M sodium dodecyl sulfate; 10% glycerol; pH 6.8) and samples were heated for 5 min at 85°C. Proteins were then reduced with 5% β-mercapto-ethanol, equal quantities separated by SDS-PAGE with precasted Mini-PROTEAN TGX Stain-Free Gels, and transferred onto PVDF membranes with the Trans-Blot Turbo Transfer System, according to the manufacturer's instructions (Bio-Rad). Total protein normalization was confirmed by Ponceau Red staining, based on the level of the large subunit of Rubisco. After incubation with 5% (w/v) nonfat milk in PBST solution (0.14 M NaCl; 0.0027 M KCl; 0.01 M PO_4^{3-}; 0.05% Tween; pH 7.4) for 60 min, the membrane was incubated in the same solution with RFP-tag primary antibody (GenScript, ref. A00682) at a 1/200 dilution for 1h at room temperature. The membrane was then washed three times for 5 min in PBST and incubated in 5% nonfat milk in PBST with horseradish peroxidase-conjugated anti-Rabbit (Agrisera, ref. AS09 602) antibody at a 1/10 000 dilution for 1h at room temperature. The membrane was then washed a further three times in PBST, developed using Clarity Max Western ECL Substrate, and imaged with a Chemidoc XRS+ System (Bio-Rad).

Measurement of photosynthetic parameters

Stromal Ca^{2+} response and photosynthetic parameters (QY: quantum yield of Photosystem II) were simultaneously measured with a Fluorescence Kinetic Microscope FC 2000-Z (FKM) (PSI, Drásov, Czech Republic) on detached cotyledons of NTRC-R-GECO1 and WT seedlings. Three custom scripts were written with the Fluorcam7 software for measuring maximum QY of PSII before HL treatment, for measuring R-GECO1 fluorescence during HL treatment, and for measuring maximum QY of PSII after HL treatment. The cotyledons were dark-adapted for 5 min before each measurement of maximum QY of PSII (see experimental design in Figure S7A). The cotyledons were imaged from the abaxial side with 30% 523 nm LED excitation light and a blue light stimulus (10% 405 nm) was provided from the adaxial side. R-GECO1 emission was collected with a Semrock FF01-593/46 nm BrightLine® single-band bandpass filter (Laser 2000). The maximum QY of PSII was calculated according to the formula (Fm-F0)/Fm, and plotted as Fv/Fm. For R-GECO1 signal quantification, average intensities of the images were calculated with Fluorcam software. The data was subtracted by the average intensity of three biological repeats of WT seedlings (background), normalized to the average baseline values, and plotted over time.

QUANTIFICATION AND STATISTICAL ANALYSIS

Statistical analyses were conducted with Graphpad Prism. For AUC and TRM, one-way ANOVA was applied at significant level $\alpha = 0.05$. When there were statistically significant differences, Fisher test was applied for mean comparisons. Error bars indicate SEM (standard error of means). For Fv/Fm, parametric paired t-test was applied at significant level $\alpha = 0.05$, medians are indicated with 95% CI (confidence interval). The numbers of independent biological replicates are indicated in the figure legends.